Available online at www.sciencedirect.com
SCIENCE DIRECT®
Journal of Loss Prevention in the Process Industries 16 (2003) 457–478
Journal of Loss Prevention in the process industries
www.elsevier.com/locate/jlp

On the determination of the laminar burning velocity from closed vessel gas explosions

A.E. Dahoe *, L.P.H. de Goey

Department of Mechanical Engineering, Eindhoven University of Technology, Den Dolech 2, Postbus 513, 5600 MB Eindhoven, The Netherlands

Abstract

A methodology to determine the laminar burning velocity from closed vessel gas explosions is explored. Unlike other methods which have been used to measure burning velocities from closed vessel explosions, this approach belongs to the category which does not involve observation of a rapidly moving flame front. Only the pressure–time curve is required as experimental input. To verify the methodology, initially quiescent methane–air mixtures were ignited in a 20-l explosion sphere and the equivalence ratio was varied from 0.67 to 1.36. The behavior of the pressure in the vessel was measured as a function of time and two integral balance models, namely, the thin-flame and the three-zone model, were fitted to determine the laminar burning velocity. Data on the laminar burning velocity as a function of equivalence ratio, pressure and temperature, measured by a variety of other methods have been collected from the literature to enable a comparison. Empirical correlations for the effect of pressure and temperature on the laminar burning velocity have been reviewed and two were selected to be used in conjunction with the thin-flame model. For the three-zone model, a set of coupled correlations has been derived to describe the effect of pressure and temperature on the laminar burning velocity and the laminar flame thickness. Our laminar burning velocities are seen to fall within the band of data from the period 1953–2003. A comparison with recent data from the period 1994–2003 shows that our results are 5–10% higher than the laminar burning velocities which are currently believed to be the correct ones for methane–air mixtures. Based on this observation it is concluded that the methodology described in this work should only be used under circumstances where more accurate methods can not be applied.

Keywords: Deflagration; Burning velocity; Flame thickness

1. Introduction

In an earlier paper (Dahoe, Zevenbergen, Lemkowitz, & Scarlett, 1996; hereafter referred to as DZLS) two integral balance models have been presented as an alternative to the well-known cube-root-law and it was demonstrated that they can be applied in two distinct ways. Firstly, they can be used to predict the pressure development of a deflagration in an enclosure when the burning velocity and the flame thickness of a particular combustible mixture are known in advance. Secondly, they can be fitted to the experimental pressure–time curve of a deflagration in a laboratory test vessel to find an estimate of the burning velocity and the flame thickness. Although the possibility of finding the burning velocity and flame thickness has indeed been demonstrated in DZLS by fitting the three-zone model to the pressure curve of a turbulent cornstarch-air explosion, little was done to explore the true potential of this approach. This was partly due to the absence of reference data on the burning velocity and the flame thickness of dust–air mixtures, partly to a deficiency in our knowledge of how these quantities behave as a function of turbulence, and partly to a lack in our understanding of how turbulent flow properties are being modified in the course of an explosion.

Since laminar gas explosions present a much simpler case, it was decided to apply the thin-flame model and

* Corresponding author. Tel.: +31-40-247-2393; fax: +31-40-2433445.
E-mail address: a.e.dahoe@tue.nl (A.E. Dahoe).

[1] The symbols used throughout this work are explained below. When a symbol represents something else than stated here, or when a symbol in the text is not explained here, or when a symbol represents more than one quantity, its precise meaning is clarified by the text.

0950-4230/$ - see front matter © 2003 Elsevier Ltd. All rights reserved.
doi:10.1016/S0950-4230(03)00073-1

Nomenclature

$\hat{C}_P$	constant pressure specific heat per unit mass (J kg^{-1} K^{-1})[1]
$\hat{C}_V$	constant volume specific heat per unit mass (J kg^{-1} K^{-1})
E_a	activation energy (J mol^{-1})
$\mathbf{f}_i$	sum of body forces per unit mass acting on the ith species (N kg^{-1})
$\mathbf{j}_h$	enthalpy flux vector (W m^{-2})
h	microscopic enthalpy per unit mass (J kg^{-1})
$h^\circ_{f_i}$	heat of formation of the ith species at reference conditions (J kg^{-1})
K_G	gas explosion severity index (bar m s^{-1})
m_u	mass of unburnt mixture (kg)
n_0	moles of gas present before explosion (mol)
n_e	moles of gas present after explosion (mol)
$\mathbf{q}$	radiant flux (W m^{-2})
p	microscopic pressure (Pa)
P	macroscopic pressure (Pa)
P_{max}	maximum explosion pressure (Pa)
r_{flame}	flame radius (m)
r_{front}	location of front edge of the flame zone (m)
r_{rear}	location of rear edge of the flame zone (m)
R	universal gas constant (J mol^{-1} K^{-1})specific gas constant (J kg^{-1} K^{-1})
S_{fl}	surface enclosing the flame zone (m^2)
$\mathbf{S}_{uL}$	laminar burning velocity (m s^{-1})
t	times
T	temperature (K)
T°	reference temperature (K)
T_f	flame temperature (K)
T_u	temperature of the unburnt mixture (K)
T_{u0}	initial temperature of the unburnt mixture (K)
$\mathbf{v}$	velocity vector (m s^{-1})
$\mathbf{V}_i$	diffusion velocity vector of the ith species (m s^{-1})
V_{fl}	volume occupied by the flame zone (m^3)
V_{vessel}	volume explosion vessel (m^3)
$\dot{\omega}_i$	source term of the ith species (kg m^{-3} s^{-1})
$\dot{\omega}_F$	average fuel consumption rate (kg m^{-3} s^{-1})
X_i	ith species mole fraction (–)
Y_i	ith species mass fraction (–)

Greek symbols

α_i	interaction parameter of the ith species (kg m^{-2} s^{-1})
γ	heat capacity ratio, $\hat{C}_P/\hat{C}_V$ (–)
δ_L	laminar flame thickness (m)
$\Delta_c H$	heat of combustion (J kg^{-1})
$\Delta_R H$	heat of reaction (J kg^{-1})
λ	thermal conductivity (W m^{-1} K^{-1})
ν'_i	stoichiometric coefficient of the ith species on the reactant side (–)
ν''_i	stoichiometric coefficient of the ith species on the product side (–)
ρ	density (kg m^{-3})
ρ_u	density of the unburnt mixture (kg m^{-3})
τ	shear stress tensor (N m^{-2})
ϕ	equivalence ratio (–)

Other symbols

D_i diffusion coefficient of the *i*th species ($m^2\ s^{-1}$)
D_{ij} binary diffusion coefficient between the *i*th and the *j*th species ($m^2\ s^{-1}$)
$(dP/dt)_{max}$ maximum rate of pressure rise ($Pa\ s^{-1}$)
M_i molecular mass of the *i*th species ($kg\ mol^{-1}$)

Dimensionless groups

Le Lewis number (–)

the three-zone model to deflagrating gas mixtures in a closed vessel with no turbulence present. Methane was chosen as the fuel because of the wide availability of experimental laminar burning velocities, air was chosen as the oxidizer, and the equivalence ratio was varied from fuel-lean ($\phi = 0.67$) to fuel-rich ($\phi = 1.36$). Quiescent methane–air mixtures at initial conditions of atmospheric pressure and room temperature were centrally ignited to deflagration in a 20-l sphere, the pressure in the explosion chamber was measured as function of time, and the two integral balance models were fitted to these pressure–time curves. The resulting laminar burning velocities are compared with literature data and the relative importance of this approach with respect to existing methods to determine the laminar burning velocity is taken into consideration.

Despite the apparent simplicity in the absence of initial turbulence there are still a number of pitfalls that require some further clarification. Firstly, there is the influence of continually varying conditions of pressure and temperature in the vessel during an explosion. After ignition, a small spherical laminar flame is formed around the ignition point. The flame propagates away from its origin by consuming reactants at the downstream side, leaving hot combustion products behind in its wake. The sudden temperature rise of the gasses passing through the flame is accompanied by a rise in the local pressure, which generates an expansion flow and causes the unburnt mixture between the flame surface and the vessel wall to be compressed. As a result, the unburnt mixture consumed by the flame at each instant of time has different pressure and temperature. The influence of varying pressure and temperature on the laminar burning velocity and the laminar flame thickness is taken into account by means of correlations.

Secondly, there is the effect of buoyancy. The buoyancy force comes into play when hot combustion products and cold reactants coexist. It becomes increasingly important during the growth of the flame and causes its shape to change from spherical to more of a mushroom shape. The influence of buoyancy was reduced to a minimum by limiting the analysis to the early part of the pressure–time curve, based on considerations described in Section 6.

Thirdly, there is the effect of baroclinic distortion of the flame which may be understood by inspecting the source term, $\nabla\rho \times \nabla p/\rho^2$, of the vorticity equation (e.g. Eq. (5) of Dahoe, Cant, Pegg, & Scarlett, 2001). Because the flame zone is a region where the density decreases rapidly in the direction towards the ignition point and the pressure is known to decrease in the opposite direction, $\nabla\rho$ and ∇p are non-zero, and it is only under the hypothetical circumstance of perfect alignment of these gradients over the entire flame surface that no vorticity will be produced. However, the slightest misalignment between these to gradients will cause the baroclinic term to act as a source of vorticity and lead to flame wrinkling. This implies that an initially spherical laminar flame has a tendency to evolve into a wrinkled flame, even in the absence of turbulence in the flow field of the unburnt mixture ahead of the flame. The onset of such instability in closed vessels, freely propagating laminar flames and vented enclosures, first as flame cracking and then as a developed cellular structures discussed by Bradley and Harper (1994), Bradley, Hicks, Lawes, Sheppard, and Woolley (1998), Gu, Haq, Lawes, and Woolley (2000), Bradley, Cresswell, and Puttock (2001), Bradley, Sheppard, Woolley, Greenhalgh, and Lockett (2000) and Haq, Sheppard, Woolley, Greenhalgh, and Lockett (2002). With stoichiometric methane–air mixtures, ignited to deflagration in a 380 mm diameter sphere, it was observed that the onset of the instability occurred when the flame reached a radius of about 20 mm (see Fig. 1 of Gu et al.). When the flame surface becomes distorted by instability, it is subjected to a stretch rate which alters the local laminar burning velocity. Additional information from photographic observation of the propagating flame is required to find the unstretched laminar burning velocity. Since this information is absent in the methodology explored in the present paper, it is reason-

able to expect a systematic difference between our laminar burning velocities and those corrected for flame stretch.

It is worthwhile to mention that various other models have been proposed which enable the determination of the burning velocity from pressure data. A comprehensive review of these models may be found in Chapter 17 of Lees (1996). Their derivation aims at the establishment of relationships between the pressure in a closed vessel, the rate of change of the pressure, the radius of the burnt gas core in the wake of the flame, the rate of change of this radius, and the burning velocity. Our thin-flame and three-zone model may be considered as an addition to this list. Another recent model by Senecal and Beaulieu (1998) also deserves to be added to the list. It is remarkable that, following a different derivation, the final expression obtained by these authors (Eq. A-16 of Senecal and Beaulieu) to calculate the value of the burning velocity from the maximum rate of pressure rise is identical to the differential equation which constitutes the thin-flame model (i.e. Eq. (1) of the present paper). An important advantage of their approach is that it gives an estimate of the turbulent burning when the maximum explosion pressure of combustible mixture is independent of turbulence. The reader may consult Dahoe, van der Nat, Braithwaite, and Scarlett (2001) for a detailed account on the sensitivity of the maximum explosion pressure to turbulence.

This paper is organized as follows. Section 2 contains a brief description of the thin-flame model and a revision of the three-zone model. A variety of correlations for the dependence of the laminar burning velocity on pressure and temperature are reviewed in Section 3. Two of these correlations, Eqs. (19) and (20), were selected and incorporated into the thin-flame model. The reasons for choosing these particular correlations are explained. Since the three-zone model involves the laminar flame thickness as well, Section 4 is devoted to the derivation of a complementary set of correlations; one for the laminar burning velocity (76) and one for the laminar flame thickness (77). A general set of correlations, (72) and (73), is first derived from the governing equations for a multi-component reactive mixture. It is subsequently shown how these correlations are constrained to avoid redundancy before their incorporation into the three-zone model. Although parts of this derivation and methodology can be found in reference works (Williams, 1985; Kuo, 1986; Turns, 1996) it was decided to include it in a comprehensive manner. The alternative, namely, to state Eqs. (72) and (73), and to leave their verification to the self-motivation of the reader would obscure the assumptions and simplifications made to arrive at the result. Section 5 contains a review of the literature data on the dependence of the laminar burning velocity of methane–air mixtures on equivalence ratio, pressure, and temperature. The correlations of the previous two sections are fitted to these data to find an estimate of their parameters for the purpose of comparison. Section 6 describes the application of the integral balance models to experimental pressure–time curves. Laminar burning velocities obtained in this manner, as well as the optimal values of the parameters contained in the correlations from Sections 3 and 4, are compared with reference material presented in Section 5. The conclusions arising from this investigation are summarized in Section 7.

2. The thin-flame model and the three-zone model

The thin-flame model, described by DZLS, is only mentioned briefly here, Its derivation results in a dynamic relationship between the pressure and the burning velocity (DZLS, Eq. (11)), based on the assumption that the flame zone is a surface where a sudden transition occurs from unburnt into burnt mixture, and that the consumption rate of unburnt mixture equals the product of the unburnt mixture density, the flame area and the burning velocity (DZLS, Eq. (5)). For the present work it is sufficient to reproduce the final result only:

$$\frac{\mathrm{d}P}{\mathrm{d}t} = \frac{3(P_{\max}-P_0)}{R_{\mathrm{vessel}}}\left[1-\left(\frac{P_0}{P}\right)^{1/\gamma}\frac{P_{\max}-P}{P_{\max}-P_0}\right]^{2/3}\left(\frac{P}{P_0}\right)^{1/\gamma}\mathbf{S}_{\mathrm{uL}}. \quad (1)$$

The three-zone model is described more extensively because it has undergone a revision after its first publication. The principal reason for reformulating the three-zone model was that it did not become identical to the thin-flame model in the limit case of zero flame thickness. The derivation of the revised model is entirely analogous to that presented in DZLS and only the modifications are presented here. Like in the earlier version, the flame zone is a region of finite width where a gradual transition occurs from unburnt to burnt mixture, which is described by expressing the fraction of unburnt mixture as a linear function of radial coordinate. Again, two cases, each consisting of three phases are distinguished during the flame propagation process. The criteria separating the cases and governing the boundaries between the various phases remain the same. What becomes different is the manner in which the consumption rate of unburnt mixture is used to establish a relationship between the pressure development and the burning velocity (compare Eqs. (2)–(8) below with Eqs. (13)–(18) of DZLS.

The consumption of unburnt mixture within the moving flame region may be expressed as

$$\frac{\mathrm{d}m_{\mathrm{u}}}{\mathrm{d}t} = \frac{\mathrm{d}}{\mathrm{d}t}\iiint_{V_{\mathrm{fl}}} \rho_{\mathrm{u}} f(r)\mathrm{d}V \quad (2)$$

Because f is formally a scalar function of location r and time t, application of the Leibnitz formula to the total time derivative of the integral lead to

$$\frac{dm_u}{dt} = \iiint_{V_{fl}} \frac{\partial[\rho_u f(r)]dr}{\partial r \quad dt} dV + \iint_{S_{fl}} \rho_u f(r)(\mathbf{v}_s \cdot \mathbf{n}) dS. \quad (3)$$

When this equation is applied to the flame region only, it states that the accumulation of unburnt mixture equals the sum of the consumption rate within the flame zone, and the influx and efflux of unburnt mixture through the flame boundaries. For the entire volume, however, one should only take the first term on the right hand side into account because the fluxes of unburnt mixture through the flame boundaries do not affect the overall amount of unburnt mixture. Hence, substitution of Eq. (3) into (DZLS, Eq. (4)) yields the following expression for the pressure evolution:

$$\frac{dP}{dt} = -\frac{P_{max} - P_0}{m_{u0}} \iiint_{V_{fl}} \frac{\partial[\rho_u f(r)]dr}{\partial r \quad dt} dV. \quad (4)$$

Relative to a fixed observer, the integration limits, i.e. the rear and front boundaries of the flame, are propagating with the flame speed. Of course, no unburnt mixture would be consumed by the flame unless we postulate the integrand of the above equation as an explicit rate of consumption. Taking notice of the fact that the cold unburnt mixture enters the flame zone from the downstream side with a velocity equal to the burning velocity and that the consumption rate of unburnt mixture scales with this velocity, it is postulated here that the rate of disappearance of reactants in the flame zone equals the product of the gradient of the fraction of unburnt mixture and the burning velocity. In terms of Eq. (4) it simply means that the integral is evaluated by an observer standing on the combustion wave and consequently dr/dt must be set equal to $-\mathbf{S}_{uL}$. Then, Eq. (4) becomes

$$\frac{dP}{dt} = \frac{P_{max} - P_0}{m_{u0}} \int_{r_{rear}}^{r_{front}} 4\pi r^2 \mathbf{S}_{uL} \left[\rho_u \frac{\partial f(r)}{\partial r} + f(r) \frac{\partial \rho_u}{\partial r} \right] dr \quad (5)$$

$$= \frac{P_{max} - P_0}{m_{u0}} \int_{r_{rear}}^{r_{front}} 4\pi r^2 \mathbf{S}_{uL} \left[\rho_u \frac{\partial f(r)}{\partial r} \right. \quad (6)$$

$$\left. + \rho_u \frac{\partial f(r) f(r)}{\partial t \quad \rho_u} \frac{\partial \rho_u}{\partial f(r)} \right] dr$$

$$= \frac{P_{max} - P_0}{m_{u0}} \int_{r_{rear}}^{r_{front}} 4\pi r^2 \rho_u \mathbf{S}_{uL} \frac{\partial f(r)}{\partial r} \left[1 + \frac{\partial \ln \rho_u}{\partial \ln f(r)} \right] dr, \quad (7)$$

which may be rewritten into

$$\frac{dP}{dt} = \frac{P_{max} - P_0}{V_{vessel}} \left(\frac{P}{P_0} \right)^{1/\gamma} 4\pi \mathbf{S}_{uL} \int_{r_{rear}}^{r_{front}} r^2 \frac{\partial f(r)}{\partial r} \left[1 \right. \quad (8)$$

$$\left. + \frac{\partial \ln \rho_u}{\partial \ln f(r)} \right] dr,$$

after application of the adiabatic compression law (DZLS, Eq. (7)).

Although the density of the unburnt mixture is known to change within the flame zone, it is assumed in the present work that $\partial \ln \rho_u / \partial \ln f(r) = 0$. With this assumption it is seen that Eq. (7) reduces to (DZLS, Eq. (6)) when the flame thickness becomes zero, and it is obvious that the three-zone model becomes identical to the thin-flame model. Expressions for the pressure evolution can be obtained by substituting Eqs. (20), (24), (28) and (32) of DZLS into Eq. (8). These are given in Table 1 and their solution is illustrated by Fig. 1. Expressions for the calculation of the flame boundaries during the various phases remain the same as those described in DZLS.

3. Empirical correlations for the effect of pressure and temperature on the laminar burning velocity

The simultaneous change in the pressure and temperature of the unburnt mixture during a closed vessel explosion makes it necessary to rely on correlations which take these effects into account. While correlations for the laminar flame thickness are scarce, many have been proposed to describe the behavior of the laminar burning velocity. Because of their simplicity and the minimal computational burden they impose, this section is restricted to correlations which express the laminar burning velocity in terms of properties of the unburnt mixture only (i.e. $\mathbf{S}_{uL} = f(T_u, P, f)$). These relationships may be classified as follows:

- Equations that separately describe the influence of pressure and temperature on the laminar burning velocity of stoichiometric methane–air mixtures.
- Correlations describing the simultaneous influence of pressure and temperature on the burning velocity of stoichiometric methane–air mixtures.
- Correlations describing the simultaneous influence of pressure, temperature and equivalence ratio.

For stoichiometric methane–air mixtures, Andrews and Bradley (1972), proposed two separate equations, namely,

$$\mathbf{S}_{uL} = 43 P^{-0.5} \ \text{cm s}^{-1} \quad (9)$$

and

$$\mathbf{S}_{uL} = 10 + 4.59 \times 10^{-5} T_u^{2.31} \ \text{cm s}^{-1}. \quad (10)$$

These relationships are recommended for the pressure range from 5 to 100 atm at room temperature and for the temperature range from 100 to 1000 K at atmospheric pressure. Smith and Agnew (1951) correlated the behavior of the burning velocity as a function of pressure with an equation of an entirely different form:

$$\frac{\mathbf{S}_{uL}}{\mathbf{S}_{uL}^{\circ}} = \exp(0.3(1 - P^{0.54})). \quad (11)$$

Table 1
Differential equations of the three-zone model for the pressure development

Case 1	$\delta_L \leq R_{vessel}$
Phase 1a	$r_{rear} = 0.0$, $r_{front} < \delta_L$
Equation	$\frac{dP}{dt} = \frac{P_{max}-P_0}{V_{vessel}}\left(\frac{P}{P_0}\right)^{1/\gamma} 4\pi \mathbf{S}_{uL} \frac{r_{front}^3}{\delta_L}$
Phase 1b	$r_{rear} = r_{front} - \delta_L$, $\delta_L \leq r_{front} < R_{vessel}$
Equation	$\frac{dP}{dt} = \frac{P_{max}-P_0}{V_{vessel}}\left(\frac{P}{P_0}\right)^{1/\gamma} 4\pi \mathbf{S}_{uL} \left[\frac{r_{front}^3 - r_{rear}^3}{\delta_L}\right]$
Phase 1c	$R_{vessel} - \delta_L \leq r_{rear} < R_{vessel}$, $r_{front} = R_{vessel}$
Equation	$\frac{dP}{dt} = \frac{P_{max}-P_0}{V_{vessel}}\left(\frac{P}{P_0}\right)^{1/\gamma} 4\pi \mathbf{S}_{uL} \left[\frac{R_{vessel}^3 - r_{rear}^3}{\delta_L}\right]$
Case 2	$\delta_L > R_{vessel}$
Phase 2a	$r_{rear} = 0.0$, $r_{front} < R_{vessel}$
Equation	Same as phase 1a
Phase 2b	$r_{rear} = 0.0$, $r_{front} = R_{vessel}$
Equation	$\frac{dP}{dt} = \frac{P_{max}-P_0}{V_{vessel}}\left(\frac{P}{P_0}\right)^{1/\gamma} 4\pi \mathbf{S}_{uL} \frac{R_{vessel}^3}{\delta_L}$
Phase 2c	$0.0 < r_{rear} \leq R_{vessel}$, $r_{front} = R_{vessel}$
Equation	Same as phase 1c

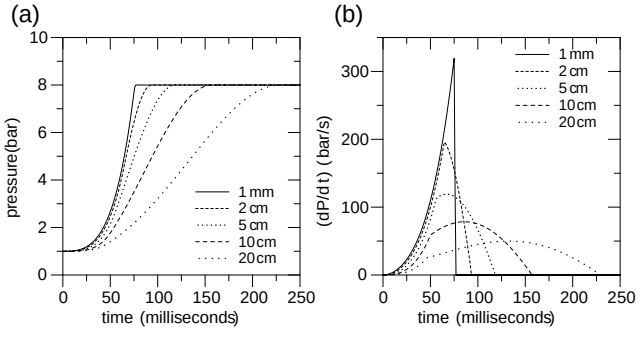

Fig. 1. Predicted pressure evolution and rate of pressure rise in a 20-l sphere and different flame thicknesses with the three-zone model. $P_0 = 1$ bar; $P_{max} = 8$ bar; $\gamma = 1.4$, $\mathbf{S}_{uL} = 0.6$ m s^{-1}.

This equation is supposed to hold for the pressure range from 0.1 to 20 atm at room temperature. Another expression for the pressure dependence of the burning velocity, valid for pressure from 0.5 to 20 atm, was given by Agnew and Graiff (1961):

$$\mathbf{S}_{uL} = 32.9 - 6.78 \ln P \ \text{cm s}^{-1}. \quad (12)$$

Barassin, Lisbet, Combourieu, and Laffitte (1967) correlated their experimental results on the effect of temperature on the burning velocity of stoichiometric methane–air mixtures as

$$\mathbf{S}_{uL} = 11 + 1.43 \times 10^{-4} T_u^{2.11} \ \text{cm s}^{-1}. \quad (13)$$

The temperature of the unburnt mixture was varied from 293 to 532 K at atmospheric pressure. Dugger (1952) investigated the effect of initial mixture temperature of stoichiometric methane–air in the temperature range from 141 to 615 K at atmosphere pressure and correlated their results as

$$\mathbf{S}_{uL} = 8 + 1.60 \times 10^{-4} T_u^{2.11} \ \text{cm s}^{-1}. \quad (14)$$

When applied to closed vessel explosions, the aforementioned relationships have the disadvantage that not all combinations of pressure and temperature, as these occur in the course of the combustion process, are covered. Clearly, correlations are needed which describe the simultaneous influence of pressure and temperature on the burning velocity. For stoichiometric methane–air mixtures at temperatures from 323 to 473 K, Babkin and Kozachenko (1966) proposed an equation,

$$\mathbf{S}_{uL} = \left(\frac{T_u}{100}\right)^2 (3.18 - 1.53^{10} \log P) \ \text{cm s}^{-1}, \quad (15)$$

for the pressure range from 1 to 23 atm and an equation,

$$\mathbf{S}_{uL} = 9.06 \left(\frac{T_u}{100}\right)^{1.47} P^{-0.646+0.509(T_u/1000)} \ \text{cm s}^{-1}, \quad (16)$$

for the pressure range from 23 to 70 atm. Perlee, Fuller, and Saul (1974) suggested that

$$\mathbf{S}_{uL} = \left(\frac{T_u}{T_{u0}}\right)^2 \left[32.9 - 6.78 \ln\left(\frac{P}{P_0}\right)\right] \ \text{cm s}^{-1}. \quad (17)$$

for stoichiometric methane–air mixtures.

There are correlations which, in addition to describing the simultaneous effect of pressure and temperature on the burning velocity, also include the influence of equivalence ratio. A system of equations for predicting the laminar burning velocity (in cm s^{-1}) for pressures from 1 to 8 atm, temperatures from 300 to 600 K, and equivalence ratios from 0.8 to 1.2 was given by Sharma, Agrawal, and Gupta (1981):

$$\mathbf{S}_{uL} = \begin{cases} C(T_u/300)^{1.68/\sqrt{\phi}} & \text{if } \phi \le 1.0 \\ C(T_u/300)^{1.68\sqrt{\phi}} & \text{if } \phi > 1.0 \end{cases} \text{ with}$$
$$C = -418 + \frac{1287}{\phi} - \frac{1196}{\phi^2} + \frac{360}{\phi^3} - 15\phi^{10}\log P. \quad (18)$$

Iijima and Takeno (1986) proposed a correlation,

$$\frac{\mathbf{S}_{uL}}{\mathbf{S}^{\circ}_{uL}} = \left(\frac{T_u}{T_{u0}}\right)^{\beta_1}\left[1 + \beta_2 \ln\left(\frac{P}{P_0}\right)\right], \quad (19)$$

which expresses the laminar burning velocity, $\mathbf{S}_{uL}(P, T_u)$, at an arbitrary pressure and temperature, in terms of the laminar burning velocity at reference conditions, $\mathbf{S}^0_{uL}(P_0,T_{u0})$. The reference temperature, T_{u0}, must be set equal to 291 K and the reference pressure, P_0, is 1 atm. The model is valid in the pressure range from 0.3 to 30 atm in combination with a temperature range from 291 to 500 K, and for an equivalence ratio in the range from 0.8 to 1.3. The dependence of the laminar burning velocity on the equivalence ratio is incorporated by means of expressions for the reference burning velocity, $\mathbf{S}^0_{uL}$, and the pressure exponents, β_1 and β_2, which are specific to the fuel. For methane–air mixtures:

$$\beta_1 = 1.60 + 0.22\,(\phi - 1) \quad (20)$$

$$\beta_2 = -0.42 - 0.31\,(\phi - 1) \quad (21)$$

$$\mathbf{S}^{\circ}_{uL} = 36.9 - 210(\phi - 1.12)^2 - 335(\phi - 1.12)^3 \text{ cm s}^{-1} \quad (22)$$

Based on experimental observations of the combustion behavior of methanol–air, iso-octane–air, and indolene–air mixtures, Metghalchi and Keck (1982) found that[2]

$$\frac{\mathbf{S}_{uL}}{\mathbf{S}^{\circ}_{uL}} = \left(\frac{T_u}{T_{u0}}\right)^{\beta_1}\left(\frac{P}{P_0}\right)^{\beta_2} \quad (23)$$

for a pressure range from 0.4 to 5.0 atm, temperatures between 298 and 700 K and equivalence ratios from 0.8 to 1.5. The reference temperature and pressure are 298 K and 1 atm. The influence of the equivalence ratio was incorporated through the temperature and pressure exponents, and through the reference burning velocity:

$$\beta_1 = 2.18 + 0.8(\phi - 1) \quad (24)$$

$$\beta_2 = -0.16 + 0.22(\phi - 1) \quad (25)$$

$$\mathbf{S}^{\circ}_{uL} = B_m + B_2(\phi - \phi_m)^2 \text{ cm s}^{-1} \quad (26)$$

Unlike Iijima and Takeno (1986), these authors observed that the pressure and temperature exponents are independent of the fuel type (within the estimated experimental error as the authors state). The reference burning velocity, however, is known to be a function of fuel type and this dependency was incorporated through the constants B_m, B_2 and ϕ_m, which are specific to fuel type.

Of all correlations reviewed in this section, Eqs. (19) and (23) are chosen to describe the influence of pressure and temperature on the laminar burning velocity. The reasons for this choice are twofold. First of all, these equations may be regarded as valid simplifications of a more general expression (see Eq. (69)) which can be derived from first principles. The second reason is that, unlike the other equations presented here, these correlations are particularly suitable for the methodology proposed in this paper because the laminar burning velocity at an arbitrary set of experimental conditions is expressed as a function of the laminar burning velocity at a particular set of reference conditions. When the latter is taken into account as a degree of freedom in an integral balance model, its magnitude can be determined by fitting the model to the pressure–time curve of a closed vessel explosion.

4. Derivation of a set of correlations for the pressure and temperature dependence of the laminar burning velocity and the laminar flame thickness

A set of correlations will now be derived for the effect of pressure and temperature on the laminar burning velocity and the laminar flame thickness by considering the Shvab–Zeldovich energy equation. This form of the energy equation can be obtained by combining the species and energy conservation equations of a multi-component reactive mixture,

$$\frac{\partial(\rho Y_i)}{\partial t} + \nabla\cdot(\rho \mathbf{v} Y_i) = -\nabla\cdot\mathbf{j}_{si} + \dot{w}_i \quad (27)$$

$$\frac{\partial(\rho h)}{\partial t} + \nabla\cdot(\rho \mathbf{v} h) = \frac{\partial p}{\partial t} + \mathbf{v}\cdot\nabla p + \tau:\nabla\mathbf{v} - \nabla\cdot\mathbf{j}_h + \sum_{i=1}^{N} \rho Y_i \mathbf{f}_i\cdot\mathbf{V}_i, \quad (28)$$

into a single expression. The flux of the ith species,

$$\mathbf{j}_{si} = \rho Y_i \mathbf{V}_i, \quad (29)$$

is stated in terms of a diffusion velocity, $\mathbf{V}_i$, and the heat flux vector,

$$\mathbf{j}_h = -\lambda\nabla T + \mathbf{q} + \sum_{i=1}^{N} \rho Y_i h_i \mathbf{V}_i + RT\sum_{i=1}^{N}\sum_{j=1}^{N}\left(\frac{X_j\alpha_i}{M_i D_{ij}}\right)(\mathbf{V}_i - \mathbf{V}_j), \quad (30)$$

[2] Notice that Eqs. (19) and (23) are related through the following series expansion:

$$a^x = 1 + \frac{x\ln a}{1!} + \frac{(x\ln a)^2}{2!} + \frac{(x\ln a)^3}{3!} + \ldots + \frac{(x\ln a)^n}{n!}.$$

is the sum of four contributions: thermal diffusion, the radiant energy flux, the Soret flux and a Dufour flux. Although both effects constitute small contributions to the overall heat balance, the Soret effect is kept in the expression for the total heat flux in order to facilitate the derivation of the Shvab–Zeldovich form of the energy equation. For a steady laminar flame, when the body forces, $\mathbf{f}_i$, the pressure gradient, ∇_p, the viscous dissipation, $\tau{:}\nabla\mathbf{v}$, and the radiant flux, $\mathbf{q}$, are neglected, and, by making use of the fact that $h = \Sigma Y_i h_i$, Eqs. (27) and (28) may be simplified to

$$\nabla\cdot[\rho Y_i(\mathbf{v} + \mathbf{V}_i)] = \dot{w}_i \tag{31}$$

$$\nabla\cdot\left[\sum_{i=1}^{N}\rho Y_i h_i(\mathbf{v} + \mathbf{V}_i) - \lambda\nabla T\right] = 0. \tag{32}$$

Since

$$h_i = h_{f_i}^{\circ} + \int_{T^{\circ}}^{T}\hat{C}_{Pi}\mathrm{d}T, \tag{33}$$

Eq. (32) may be rewritten into

$$\nabla\cdot\left[\sum_{i=1}^{N}\rho Y_i(\mathbf{v} + \mathbf{V}_i)h_{f_i}^{\circ} + \sum_{i=1}^{N}\rho Y_i(\mathbf{v} + \mathbf{V}_i)\int_{T^{\circ}}^{T}\hat{C}_{Pi}\mathrm{d}T - \lambda\nabla T\right] = 0, \tag{34}$$

which upon application of Eq. (31) to the first term on the left hand side becomes

$$\nabla\cdot\left[\rho\mathbf{v}\sum_{i=1}^{N}\int_{T^{\circ}}^{T}Y_i\hat{C}_{Pi}\mathrm{d}T + \rho\sum_{i=1}^{N}Y_i\mathbf{V}_i\int_{T^{\circ}}^{T}\hat{C}_{Pi}\mathrm{d}T - \lambda\nabla T\right] = -\sum_{i=1}^{N}h_{f_i}^{\circ}\dot{w}_i. \tag{35}$$

When air is used as the oxidizer, it is as if the combustion reactions occur in nitrogen as a background fluid and hence the diffusion velocity may be described by Fick's law:

$$\rho Y_i\mathbf{V}_i = -\rho\mathbb{D}\nabla Y_i. \tag{36}$$

Application of Fick's law to Eq. (35), and use of the fact that $\hat{C}_P = \Sigma Y_i\hat{C}_P$, leads

$$\nabla\cdot\left[\rho\mathbf{v}\int_{T^{\circ}}^{T}\hat{C}_P\mathrm{d}T - \rho\mathbb{D}\sum_{i=1}^{N}(\nabla Y_i)\int_{T^{\circ}}^{T}\hat{C}_{Pi}\mathrm{d}T - \lambda\nabla T\right] = -\sum_{i=1}^{N}h_{f_i}^{\circ}\dot{w}_i, \tag{37}$$

which can be rewritten into

$$\nabla\cdot\left[\rho\mathbf{v}\int_{T^{\circ}}^{T}\hat{C}_P\mathrm{d}T - \rho\mathbb{D}\nabla\int_{T^{\circ}}^{T}\hat{C}_{Pi}\mathrm{d}T + \rho\hat{C}_P\mathbb{D}\nabla T - \lambda\nabla T\right] = -\sum_{i=1}^{N}h_{f_i}^{\circ}\dot{w}_i, \tag{38}$$

or equivalently,

$$\nabla\cdot\left[\rho\mathbf{v}\int_{T^{\circ}}^{T}\hat{C}_P\mathrm{d}T - \rho\mathbb{D}\nabla\int_{T^{\circ}}^{T}\hat{C}_{Pi}\mathrm{d}T + \rho\hat{C}_P\mathbb{D}[1 - Le]\nabla T\right] = -\sum_{i=1}^{N}h_{f_i}^{\circ}\dot{w}_i, \tag{39}$$

because

$$\begin{aligned}\nabla\int_{T^{\circ}}^{T}\hat{C}_P\mathrm{d}T &= \nabla\sum_{i=1}^{N}Y_i\int_{T^{\circ}}^{T}\hat{C}_{Pi}\mathrm{d}T\\ &= \sum_{i=1}^{N}(\nabla Y_i)\int_{T^{\circ}}^{T}\hat{C}_{Pi}\mathrm{d}T + \sum_{i=1}^{N}Y_i\nabla\int_{T^{\circ}}^{T}\hat{C}_{Pi}\mathrm{d}T\\ &= \sum_{i=1}^{N}(\nabla Y_i)\int_{T^{\circ}}^{T}\hat{C}_{Pi}\mathrm{d}T + \sum_{i=1}^{N}Y_i\hat{C}_{Pi}\nabla T\\ &= \sum_{i=1}^{N}(\nabla Y_i)\int_{T^{\circ}}^{T}\hat{C}_{Pi}dT + \hat{C}_P\nabla T.\end{aligned} \tag{40}$$

Up to Eq. (39) none of the physical properties were assumed constant and no simplifying assumptions have been made regarding the specific heats of the individual species. The so-called Shvab–Zeldovich energy equation is obtained by setting the Lewis number, *Le*, in Eq. (39) equal to unity:

$$\nabla\cdot\left[\rho\mathbf{v}\int_{T^{\circ}}^{T}\hat{C}_P\mathrm{d}T - \rho\mathbb{D}\nabla\int_{T^{\circ}}^{T}\hat{C}_P\mathrm{d}T\right] = -\sum_{i=1}^{N}h_{f_i}^{\circ}\dot{w}_i. \tag{41}$$

Since the specific heat is known to be a weak function of temperature, it may be treated as a constant. An immediate consequence of the unity Lewis number assumption is that $\rho\mathbb{D}$ may be replaced by $\lambda/\hat{C}_P$. The continuity equation (see Fig. 2),

$$\rho_u\mathbf{v} = -\rho_u\mathbf{S}_{uL}, \tag{42}$$

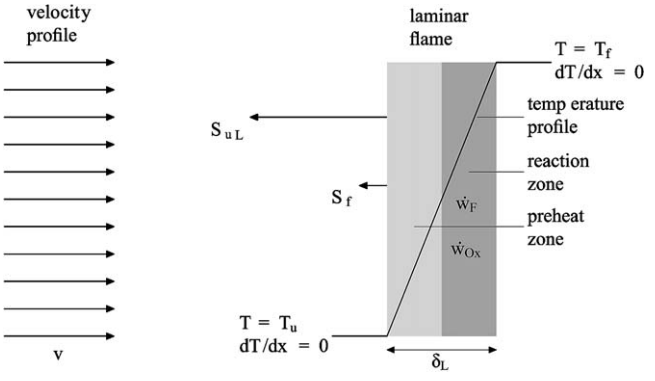

Fig. 2. Simplified structure of a premixed laminar flame.

then implies that Eq. (41) may be simplified to

$$\rho_u \hat{C}_P \mathbf{S}_{uL} \nabla T + \nabla\cdot[\lambda \nabla T] = -\sum_{i=1}^{N} h^{\circ}_{f_i} \dot{w}_i. \quad (43)$$

If the overall combustion reaction is represented by

$$1 \text{ kg Fuel} + \nu \text{ kg Oxidizer} \rightarrow (\nu + 1) \text{ kg Products}, \quad (44)$$

then

$$-\dot{w}_F = -\frac{1}{\nu}\dot{w}_O = \frac{1}{\nu+1}\dot{w}_{Pr} \quad (45)$$

and hence,

$$\sum_{i=1}^{N} h^{\circ}_{f_i}\dot{w}_i = h^{\circ}_{f_F}\dot{w}_F + h^{\circ}_{f_O}\dot{w}_O + h^{\circ}_{f_{Pr}}\dot{w}_{Pr} \quad (46)$$

$$= (h^{\circ}_{f_F} + \nu h^{\circ}_{f_O} - (\nu+1)h^{\circ}_{f_{Pr}})\dot{w}_F \quad (47)$$

$$= \Delta_c H \dot{w}_F, \quad (48)$$

where $\Delta_c H$ denotes the fuel's heat of combustion. For the laminar flame under consideration, Eq. (43) then simplifies to

$$\rho_u \hat{C}_P \mathbf{S}_{uL} \frac{dT}{dx} + \frac{d}{dx}\left(\lambda \frac{dT}{dx}\right) = -\nabla_c H \dot{w}_F. \quad (49)$$

Following the procedure described by Turns (1996) and Spalding (1979) the above differential equation may be integrated twice with the boundary conditions as dictated by the assumed temperature profile shown in Fig. 2. The first integration is performed over the entire physical domain with the boundary conditions,

$$x \rightarrow -\infty: \quad T = T_u \quad \frac{dT}{dx} = 0 \quad (50)$$

$$x \rightarrow \infty: \quad T = T_f \quad \frac{dT}{dx} = 0, \quad (51)$$

and gives:

$$\rho_u \hat{C}_P \mathbf{S}_{uL} T|_{T_u}^{T_f} + \lambda \left.\frac{\partial T}{\partial x}\right|_{dT/dx=0}^{dT/dx=0} = -\Delta_c H \int_{-\infty}^{\infty} \dot{w}_F dx. \quad (52)$$

When the assumed temperature profile is used to apply a change of variables,

$$\frac{\partial T}{\partial x} = \frac{T_f - T_u}{\delta_L} \Leftrightarrow dx = \frac{\delta_L}{T_f - T_u} dT, \quad (53)$$

Eq. (52) transforms into

$$\rho_u \hat{C}_P \mathbf{S}_{uL}(T_f - T_u) = -\frac{\delta_L \Delta_c H}{T_f - T_u}\int_{T_u}^{T_f} \dot{w}_F dT = \quad (54)$$

$$-\delta_L \Delta_c \bar{\dot{w}}_F$$

where $\bar{\dot{\omega}}_F$ denotes the average fuel consumption rate. This results in a single algebraic equation,

$$\rho_u \hat{C}_P \mathbf{S}_{uL}(T_f - T_u) + \delta_L \Delta_c H \bar{\dot{w}}_F = 0 \quad (55)$$

with two unknowns, namely, the laminar burning velocity, $\mathbf{S}_{uL}$, and the laminar flame thickness, δ_L. Notice that this equation requires that the heat production in the reaction zone is balanced by the heat absorption of the incoming unburnt mixture. In order to obtain explicit expressions for $\mathbf{S}_{uL}$ and δ_L, it is necessary to find a second equation. This is done by repeating the integration procedure with the following boundary conditions:

$$x \rightarrow -\infty: \quad T = T_u \quad \frac{dT}{dx} = 0 \quad (56)$$

$$x = \frac{\delta_L}{2}: \quad T = \frac{T_u + T_f}{2} \quad \frac{dT}{dx} = \frac{T_f - T_u}{\delta_L}. \quad (57)$$

This leads to the following integrated form of Eq. (49):

$$\rho_u \hat{C}_P \mathbf{S}_{uL} T|_{T_u}^{(T_u+T_f)/2} + \lambda \left.\frac{\partial T}{\partial x}\right|_{dT/dx=0}^{(T_f-T_u)/\delta_L} = \quad (58)$$

$$-\Delta_c H \int_{-\infty}^{\delta_L/2} \dot{w}_F dx,$$

which simplifies into

$$\frac{1}{2}\rho_u \hat{C}_P \mathbf{S}_{uL}(T_f - T_u) - \lambda \frac{T_f - T_u}{\delta_L} = 0, \quad (59)$$

since $\dot{\omega}_F$ is practically zero in the preheat zone. This equation state that the required energy flux for heating the unburnt mixture to the flame temperature is controlled by the conduction of heat through the preheat zone.

The desired expressions for $\mathbf{S}_{uL}$ and δ_L can then be obtained by solving Eqs. (55) and (59):

$$\mathbf{S}_{uL} = \left[-2\frac{\lambda}{\rho_u \hat{C}_P}\frac{\Delta_c H}{\hat{C}_P (T_f - T_u)}\frac{\bar{\dot{w}}_F}{\rho_u}\right]^{1/2} \quad (60)$$

$$\delta_L = \left[-2\frac{\lambda}{\rho_u \hat{C}_P}\frac{\hat{C}_P (T_f - T_u)}{\Delta_c H}\frac{\rho_u}{\bar{\dot{w}}_F}\right]^{1/2}. \quad (61)$$

Since the heat of combustion of the fuel relates to the temperature of the product mixture as $\Delta_c H = (\nu + 1)\hat{C}_P(T_f - T_u)$, these relationships may also be stated as

$$\mathbf{S}_{uL} = \left[-2\frac{\lambda}{\rho_u \hat{C}_P}(\nu+1)\frac{\bar{\dot{w}}_F}{\rho_u}\right]^{1/2} \quad (62)$$

$$\delta_L = \left[-2\frac{\lambda}{\rho_u \hat{C}_P}\frac{1}{\nu+1}\frac{\rho_u}{\bar{\dot{w}}_F}\right]^{1/2}. \quad (63)$$

Notice that the factor 2 in these equations results from the choice of the width of the preheat zone. A wider or

thinner preheat zone would have resulted in a different value. It is assumed that this arbitrariness is largely canceled in the establishment of Eqs. (72) and (73).

The effect of pressure and temperature can now be incorporated as follows. With an assumed generalized reaction,

$$\sum_{i=1}^{N} \nu'_i \mathrm{M}_i \rightarrow \sum_{i=1}^{N} \nu''_i \mathrm{M}_i, \tag{64}$$

and an overall reaction order of $n = \Sigma_{i=1}^{N} \nu'_i$, the mass consumption rate of each individual species may be stated as:

$$\frac{\mathrm{d}(\rho Y_i/\mathrm{M}_i)}{\mathrm{d}t} = (\nu''_i - \nu'_i) B T^m \exp\left(-\frac{E_a}{RT}\right) \prod_{j=1}^{N} \left(\frac{\rho Y_j}{\mathrm{M}_j}\right)^{\nu'_j}, \tag{65}$$

where the constants m and E_a, respectively, denote the temperature exponent of the pre-exponential factor and the activation energy. Hence,

$$\bar{\dot{\omega}}_F \propto \rho^n B T^m \exp\left(-\frac{E_a}{RT}\right) \prod_{j=1}^{N} (Y_j/\mathrm{M}_j)^{\nu'_j}, \tag{66}$$

and since

$$\rho_u \propto T_u^{-1} P, \tag{67}$$

while most of the combustion occurs in the reaction zone, the average fuel consumption rate is found to scale as follows:

$$\bar{\dot{\omega}}_F \propto T_f^{-n} P^n T_f^m \exp\left[-\frac{E_a}{RT_f}\right]. \tag{68}$$

Substitution of the two preceding relationships into Eqs. (62) and (63) gives the following scalings for the laminar burning velocity and the laminar flame thickness:

$$\frac{\mathbf{S}_{uL}}{\mathbf{S}^\circ_{uL}} \propto \sqrt{\frac{\lambda(T_u)}{\lambda(T_{u0})}} \frac{T_u}{T_{u0}} \left(\frac{P}{P_0}\right)^{(n-2)/2} \left(\frac{T_f}{T_f^\circ}\right)^{-(n/2)} \left(\frac{T_f}{T_f^\circ}\right)^{m/2} \exp\left[-\frac{E_a}{2R}\left(\frac{1}{T_f} - \frac{1}{T_f^\circ}\right)\right] \tag{69}$$

$$\frac{\delta_L}{\delta^\circ_L} \propto \sqrt{\frac{\lambda(T_u)}{\lambda(T_{u0})}} \left(\frac{P}{P_0}\right)^{-(n/2)} \left(\frac{T_f}{T_f^\circ}\right)^{n/2} \left(\frac{T_f}{T_f^\circ}\right)^{-(m/2)} \exp\left[+ \frac{E_a}{2R}\left(\frac{1}{T_f} - \frac{1}{T_f^\circ}\right)\right], \tag{70}$$

where $\mathbf{S}^\circ_{uL}$, δ°_L and T_f° are the laminar burning velocity, the laminar flame thickness and the flame temperature of the unburnt mixture at a reference state P_0 and T_{u0}. The thermal conductivity is a function of the temperature of the preheat zone and should in fact be expressed as a function of the average preheat zone temperature, $T_u + 1/2(T_f - T_u)$. Since the flame temperature is hardly affected by the temperature of the unburnt mixture, the thermal conductivity is expressed here as a function of the temperature of the unburnt mixture only.

Owing to the fact that the unburnt mixture at the downstream side of the flame undergoes adiabatic compression during an explosion in a closed vessel, the pressure and temperature of the unburnt mixture do not behave independently from each other. Instead, they are correlated according to the adiabatic compression law,

$$\frac{T_u}{T_{u0}} = \left(\frac{P}{P_0}\right)^{(\gamma-1)/\gamma}, \tag{71}$$

where γ denotes the specific heat ratio. When Eqs. (69) and (70) are rewritten as

$$\frac{\mathbf{S}_{uL}}{\mathbf{S}^\circ_{uL}} \propto \sqrt{\frac{\lambda(T_u)}{\lambda(T_{u0})}} \frac{T_u}{T_{u0}} \left(\frac{P}{P_0}\right)^{-1} \left(\frac{T_f}{T_f^\circ}\right)^{-(n-m)/2} \left(\frac{P}{P_0}\right)^{n/2} \exp\left[-\frac{E_a}{2R}\left(\frac{1}{T_f} - \frac{1}{T_f^\circ}\right)\right] \tag{72}$$

$$\frac{\delta_L}{\delta^\circ_L} \propto \sqrt{\frac{\lambda(T_u)}{\lambda(T_{u0})}} \left(\frac{T_f}{T_f^\circ}\right)^{(n-m)/2} \left(\frac{P}{P_0}\right)^{-(n/2)} \exp\left[+ \frac{E_a}{2R}\left(\frac{1}{T_f} - \frac{1}{T_f^\circ}\right)\right], \tag{73}$$

substitution of the adiabatic compression law (71) and the following assumptions[3],

$$\sqrt{\frac{\lambda(T_u)}{\lambda(T_{u0})}} \propto \left(\frac{T_u}{T_{u0}}\right)^{\alpha_1} \tag{74}$$

$$\left(\frac{T_f}{T_f^\circ}\right)^{-(n-m)/2} \exp\left[-\frac{E_a}{2R}\left(\frac{1}{T_f} - \frac{1}{T_f^\circ}\right)\right] \propto \left(\frac{P}{P_0}\right)^{\alpha_2}, \tag{75}$$

leads to

$$\frac{\mathbf{S}_{uL}}{\mathbf{S}^\circ_{uL}} \propto \left(\frac{P}{P_0}\right)^{c+(\gamma-1)/\gamma-1+\alpha} \tag{76}$$

$$\frac{\delta_L}{\delta^\circ_L} \propto \left(\frac{P}{P_0}\right)^{c-\alpha}, \tag{77}$$

where c denotes a mixture specific constant. These are the correlations for the effect of pressure and temperature on the laminar burning velocity and the laminar flame thickness to be used in conjunction with the three-zone model.

---

[3] The temperature dependence of the thermal conductivity is described by the Sutherland equation (Vasserman, Kazavchinskii, & Rabinovich, 1971: p. 311),

$$\frac{\lambda(T)}{\lambda(T_0)} = \left(\frac{T_0 + C}{T + C}\right)\left(\frac{T}{T_0}\right)^{3/2}$$

where C denotes the Sutherland constant which must be determined experimentally for each substance. It is assumed that this relationship may be approximated by Eq. (74).

Assumption (75) requires some further clarification. For a constant-pressure flame, for example, the law of conservation of energy requires the total enthalpy per unit mass of mixture to remain constant throughout the flame zone. This may be expressed by

$$\sum_{i=1}^{N}\left[Y_{ui}h_{f_i}^{\circ} + Y_{ui}\int_{T^{\circ}}^{T^{u}}\hat{C}_{Pi}\mathrm{d}T\right] = \sum_{i=1}^{N}\left[Y_{bi}h_{fi}^{\circ} + Y_{bi}\int_{T^{\circ}}^{T^{f}}\hat{C}_{Pi}\mathrm{d}T\right], \quad (78)$$

where Y_{ui} and Y_{bi} denote the mass fractions of the species that, respectively, constitute the unburnt and the burnt mixture. When this equation is rewritten as

$$\sum_{i=1}^{N} Y_{ui}\hat{C}_{Pi}(T_u - T^{\circ}) - \Delta_R H = \sum_{i=1}^{N} Y_{bi}\hat{C}_{Pi}(T_f - T^{\circ}), \quad (79)$$

where

$$\Delta_R H = \sum_{i=1}^{N}(Y_{bi} - Y_{ui})h_{f_i}^{\circ} \quad (80)$$

denotes the heat of reaction per mass unit, it is obvious that an increase in T_u will have little effect on T_f since $\Sigma Y_{ui}\hat{C}_{Pi}(T_u - T^{\circ}) \ll \Delta_R H$. Eq. (79) also clarifies the influence of pressure on the flame temperature. If dissociation occurs to a significant degree within the reaction zone, a chemical equilibrium exists between the reaction products and their subsequent dissociation products. Changes in the system pressure will alter the mass fractions of the burnt mixture, Y_{bi}, and since the left hand side of Eq. (79) is practically independent of pressure, a change in the species mass fractions can only be balanced by a change of T_f. It is known that, the hotter the flame, the larger the degree of dissociation, and the more sensitive the flame temperature becomes to variations in the system pressure. Due to the comparatively low flame temperature of methane–air mixtures[4] dissociation, and hence the effect of pressure on the flame temperature, is considered to be of minor importance. It is nevertheless assumed that the effect of pressure on the flame temperature must be taken into account by Eq. (75).

5. Literature data on the effect of equivalence ratio, pressure and temperature on the laminar burning velocity

The aim of this section is to find estimates for the effect of equivalence ratio, pressure and temperature on the laminar burning velocity. Experimental and calculated burning velocities reported by other researchers are interpreted here on the basis of correlations presented in the previous two sections.

Fig. 3 shows the variation of the laminar burning velocity as a function of the equivalence ratio. One may observe a variation of about 10 cm s^{-1} between the 16 different data sets when the equivalence ratio ranges from the lower flammability limit to the stoichiometric concentration, and this discrepancy increases as the upper flammability limit is approached. This large factor of uncertainty may be ascribed to the variety of methods that have been used to determine the magnitude of this quantity. The laminar burning velocities obtained in our work will be compared with these results.

The literature data on the effect of pressure on the laminar burning velocity of stoichiometric methane–air mixtures (see Fig. 4) imply a weak dependence as a function of pressure. The laminar burning velocity changes by a factor of 20 (from 100 to 5 cm s^{-1}) when the pressure is changed by a factor of 1000 (from 0.1 to 100 bar). The experimental results from 14 different data sets in Fig. 4 also indicate that the overall reaction order does not remain constant over the entire pressure range and that there are discrepancies between the results obtained by different experimental methods. These discrepancies are more pronounced for pressures lower than

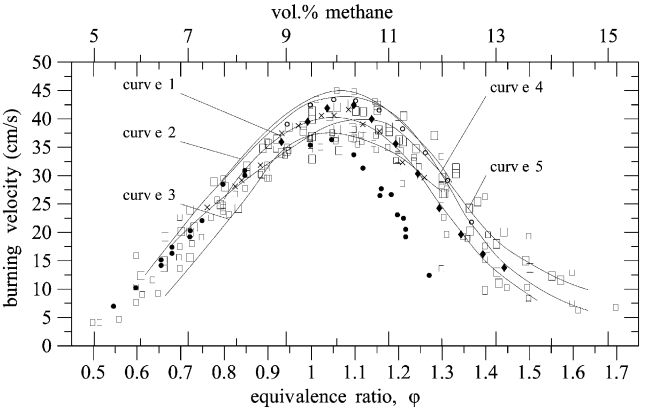

Fig. 3. Effect of equivalence ratio on the laminar burning velocity of methane–air mixtures, $P = 1$ bar, $T = 288.15$–298.15 K. × Clingman, Brokaw, and Pease (1953), ● Karpov and Sokolik (1961), △ Barassin et al. (1967), ○ Lindow (1968), ▽ Edmondson and Heap (1969), □ Edmondson and Heap (1970), ◇ Reed, Mineur, and McNaughton (1971), ☒ Andrews and Bradley (1972), ▲ Günther and Janisch (1972), ⊞ van Maaren et al. (1994), ⊕ Clarke, Stone, and Beckwith (1995), ★ Wu and Law (1984), ⊟ Iijima and Takeno (1986), ⊗ Kawakami, Okajima, and Iinuma (1988), ∗ Egolfopoulos, Cho, and Law (1989), ● *Flamelet Library*, curve 1: Scholte and Vaags (1959), curve 2: Gibbs and Calcote (1959), curve 3: Egerton and Lefebvre (1954), curve 4: Warnatz (1981), curve 5: Tsatsaronis (1978).

[4] The final temperature of the burnt mixture can be estimated from the explosion pressure since $P_e/P_0 = (n_e/n_0)/(T_f/T_0)$ where n_0 and n_e denote the total number of moles of gas present, before and after the explosion. Stoichiometric methane–air mixtures gave an explosion pressure of 8.7 bar (see Fig. 6). Air consists for 79% of inert nitrogen and the stoichiometric methane–oxygen reaction, $CH_4 + 2O_2 \rightarrow CO_2 + 2H_2O$, conserves the amount of gas. Therefore, $n_e = n_0$ and the temperature of the burnt mixture is found to be 2610 K.

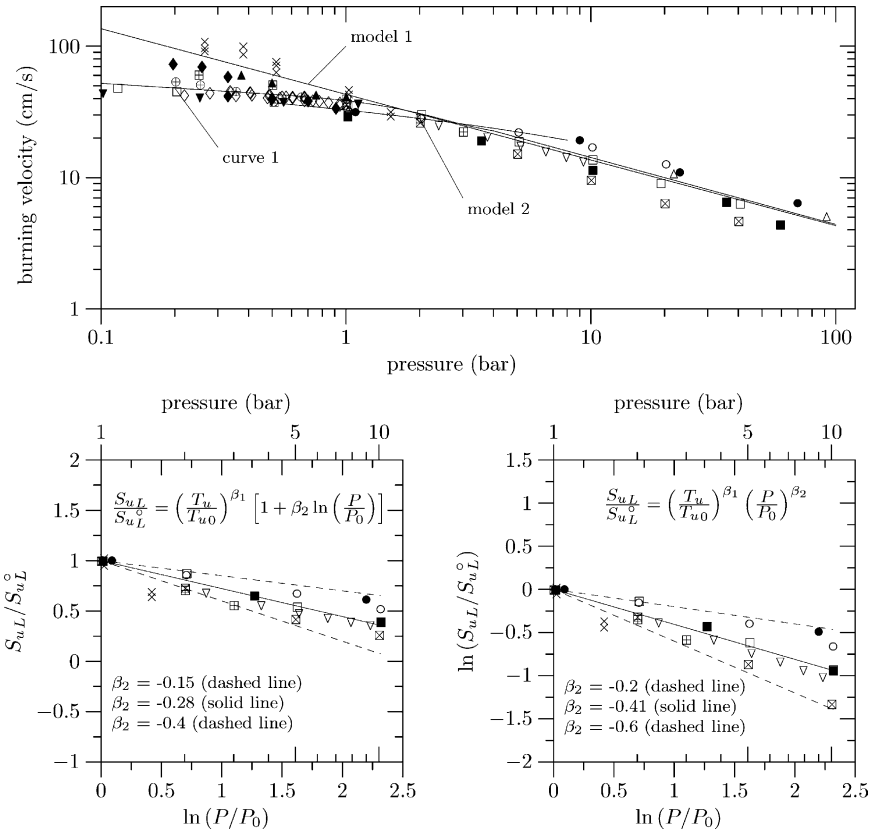

Fig. 4. Effect of pressure on the laminar burning velocity of stoichiometric methane–air mixtures, T = 288.15–298.15 K. ▽ Egerton and Lefebvre (1954), □ Diederichsen and Wolfhard (1956), ▲ Clingman and Pease (1956), ▼ Manton and Milliken (1956), ◆ Singer, Grumer, and Cook (1956), ◇ Gilbert (1957) (luminous zone), ⊕ Gilbert (1957) (wire shadow), △ Strauss and Edse (1959), ○ Agnew and Graiff (1961), ● Babkin and Kozachenko (1966), × Bradley and Hundy (1971), ■ Babkin, Kozachenko, and Kuznetsov (1964), ⊞ Egolfopoulos et al. (1989), ⊠ *Flamelet Library*, curve 1: Tsatsaronis (1978), model 1: Eq. (9) by Andrews and Bradley (1972), model 2: Eq. (18) by Sharma et al. (1981).

1 bar. To minimize these inaccuracies only literature data in the pressure range of 1–10 bar are used. Each data set was re-scaled by dividing it by the value of the laminar burning velocity at reference conditions, and this ratio is plotted in accordance with Eqs. (19) and (23), as shown in the lower part of Fig. 4, so that the slope of these data corresponds to the pressure exponent, β_2, in these equations. The value of β_2 found by means of fitting the thin-flame model and the three-zone model can then be compared with the value of the slope. The solid line in the lower-left part of Fig. 4 indicates that the pressure exponent of Eq. (19) has a value of -0.28, but the dashed lines indicate that this pressure exponent may vary between -0.15 and -0.4 from one method of determination to another. The lower-right part of the figure indicates that the pressure exponent of Eq. (23) has a value of -0.41, but that it can vary between -0.2 and -0.6.

With hydrocarbon–air mixtures, it is generally observed that $\mathbf{S}_{uL} \propto T^{\beta_1}$ where the exponent β_1 ranges between 1.5 and 2. The temperature exponent in Eqs. (19) and (23) can be determined by re-scaling the literature data in the upper part of Fig. 5 as shown by the lower part of the same figure. From the latter, one may deduce a value of 1.89 (the slope of the solid line) for the temperature exponent. The dashed lines, with slopes of 1.5 and 2.2, reflect the considerable scatter in both the magnitude of the laminar burning velocities, as well as in their rate of increase with temperature.

The lower-right part of Fig. 5 may also be used to estimate the values of c and α in Eqs. (76) and (77). From the slope of these data and Eq. (69) one may conclude that

$$\sqrt{\frac{\lambda(T_u)}{\lambda(T_{u0})}} \propto \left(\frac{T_u}{T_{u0}}\right)^{\beta_1 - 1} \propto \left(\frac{P}{P_0}\right)^{(\beta_1 - 1)((\gamma-1)/\gamma)} \propto \left(\frac{P}{P_0}\right)^{c}. \tag{81}$$

When the value of γ is taken to be 1.4, one finds that c = 0.25 with β_1 = 1.89, and that c varies between 0.14 and 0.34 on the basis of the slopes of the dashed lines. An estimation of the value of α can be obtained as follows. Dryer and Glassman (1972) proposed the following expression (which is considered to be outdated by some researchers but nevertheless suitable for our

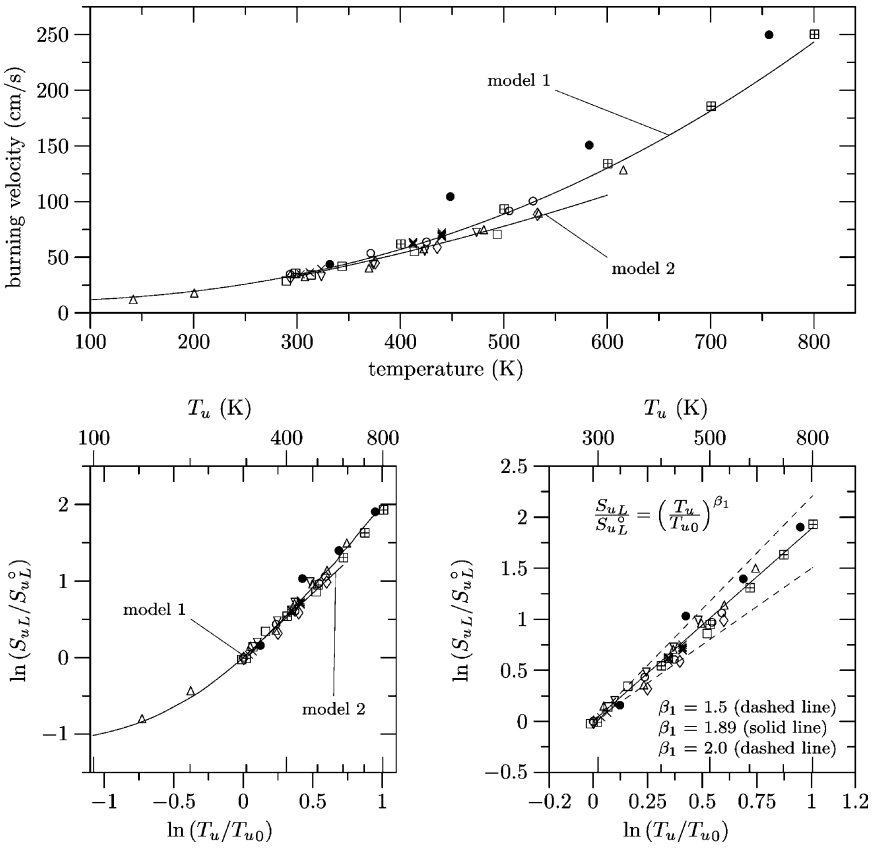

Fig. 5. Effect of temperature on the laminar burning velocity of stoichiometric methane–air mixtures, $P = 1$ bar. ● Johnston (1947), △ Dugger (1952), × Halpern (1958), □ Babkin et al. (1964), ▽ Babkin and Kozachenko (1966), ◇ Barassin et al. (1967) (tube), ○ Barassin et al. (1967) (burner), ⊞ *Flamelet Library*, model 1: Eq. (10) by Andrews and Bradley (1972), model 2: Eq. (18) by Sharma et al. (1981).

purpose) for the methane–oxygen reaction which fits their experimental data,

$$\frac{\mathrm{d[CH_4]}}{\mathrm{d}t} = 10^{13.2\pm0.20}\exp\left[\frac{(-48400 \pm 1200)}{RT}\right][\mathrm{CH_4}]^{0.7}[\mathrm{O_2}]^{0.8}\ \mathrm{mole\ cm^{-3}\ s^{-1}}, \quad (82)$$

(R in cal mol^{-1} K^{-1}). Since the overall reaction order is equal to the sum of the exponents of the reactant concentrations, this expression implies that the methane–oxygen reaction has an overall reaction order of 1.5. On the assumption that the flame temperature is not affected by pressure and temperature, substitution of this value into Eq. (72) in combination with the estimates for c in Eq. (76) indicates that α must have a value close to 0.5 and that it must be in the range from 0.41 to 0.61.

6. Determination of the laminar burning velocity from closed vessel deflagrations

This section describes how the thin-flame model and the three-zone model can be used to find the laminar burning velocity from the pressure–time curve of a deflagration in a closed vessel. For this purpose, a number of gas explosions were carried out in the strengthened 20-l sphere described in Dahoe et al. (1995) and Dahoe (2000). All experiments were carried out with quiescent methane–air mixtures at initial conditions of 1 bar and 298.15 K, and the equivalence ratio was varied from 0.67 to 1.36. A spark was used to ignite the mixtures at the center of the vessel to deflagration. The experimental pressure–time curves are shown in Fig. 6. In all experiments, the pressure is seen to behave as follows. After ignition, the pressure in the explosion vessel increases progressively until the rate of pressure rise achieves a maximum (the maximum rate of pressure rise, $(\mathrm{d}P/\mathrm{d}t)_{\max}$) and continues to increase towards a maximum (the maximum explosion pressure, $P_{\max}$) with a decreasing rate of pressure rise. After completion of the explosion, the pressure is seen to decrease. To enable a comparison between our measurements and work by other researchers, the explosion severity parameters ($P_{\max}$ and $(\mathrm{d}P/\mathrm{d}t)_{\max}$) of our explosion curves are presented together with values reported by Cashdollar and Hertzberg (1985) in the lower part of Fig. 6. These authors used a 20-l explosion vessel which was not spherical, but consisted of a cylinder with a hemispherical bottom and top. Our explosion severity parameters are found to be in agreement with those of Cashdollar

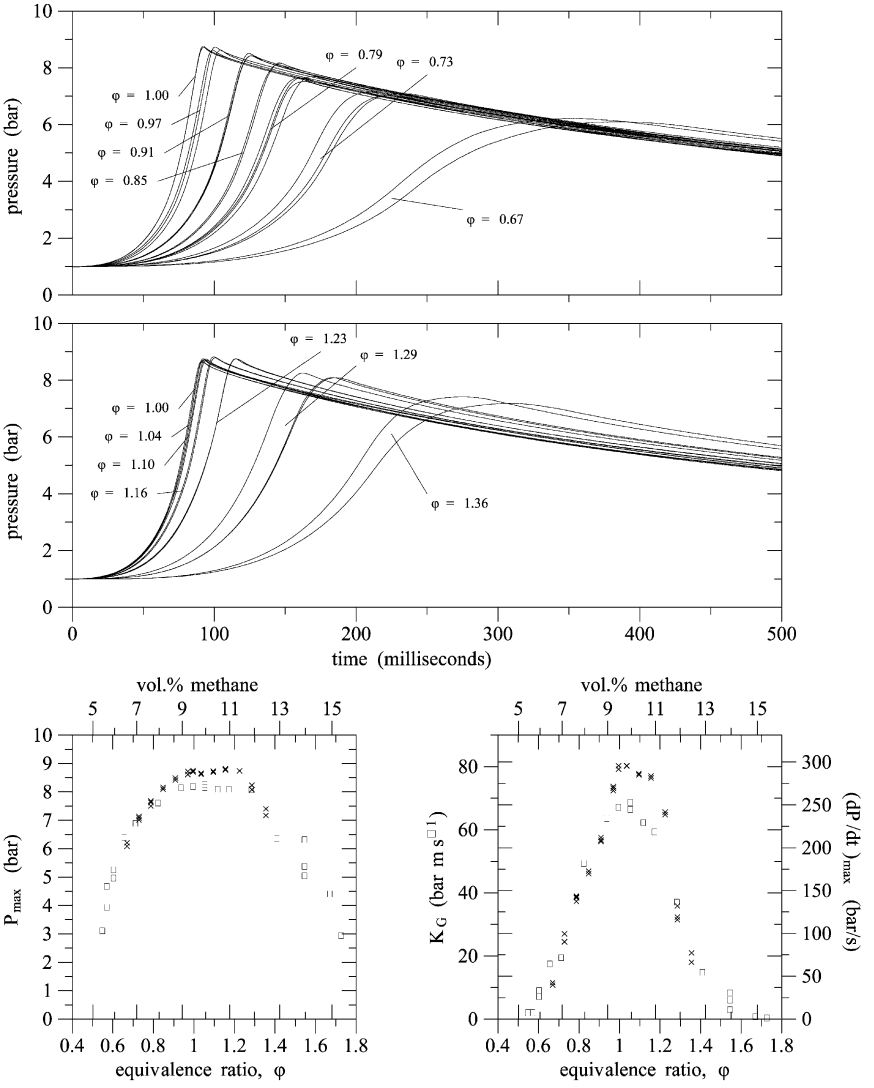

Fig. 6. Measured explosion pressure curves of fuel lean to stoichiometric methane–air mixtures, the maximum explosion pressure, the maximum rate of pressure rise, and K_G values (× our results, ■ Cashdollar & Hertzberg, 1985).

and Hertzberg for off-stoichiometric mixtures, but differences may be observed with near-stoichiometric mixtures. With stoichiometric mixtures, discrepancies of 6% and 13% are observed in P_{max} and $(dP/dt)_{max}$. Bartknecht (1981) measured the explosion behavior of stoichiometric methane–air mixtures in a 20-l explosion sphere and found a P_{max} of 8.4 bar and a K_G value[5] of 55 bar m s^{-1}. Our measurements show that for stoichiometric methane–air mixtures, P_{max} is 8.7 bar and K_G is 80 bar m s^{-1}.

The occurrence of an inflection point in all our pressure–time curves is attributed to the effect of buoyancy. Due to the density difference between the hot combustion products and the cold unburnt mixture, a flame ball accelerates in the upward direction while reactants are being consumed by the expanding flame surface. During this process, the pressure in the vessel increases with an increasing rate of pressure rise until the upper part of the flame reaches the wall. From this point onwards, there is still an amount of unburnt mixture is being consumed by the lower part of the flame. As this remainder of unburnt mixture is being consumed, the flame area decreases. Hence the decrease of the rate of pressure rise and the occurrence of an inflection point. If the thin-flame model and the three-zone model were to be fitted to the entire explosion curve, this process would bias the optimal

[5] The K_G value, also known as the gas explosions severity index, is a quantity which forms the design basis of a great deal of practical safety measures. It is defined as the product of the maximum rate of pressure rise and the cube-root of the volume of the explosion vessel, $K_G = (dP/dt)_{max} V_{1/3}$, and believed to be a mixture specific explosion severity index. The K_G value was defined in this way because it was believed that maximum rates of pressure rise measured in differently sized vessels would become volume-invariant if they were multiplied by the cube-root of the volume. The practical significance of this quantity rests on the assumption that once it is known for a particular mixture from an experiment in a small laboratory test vessel, the maximum rate of pressure rise in a larger industrial vessel is predicted correctly by dividing it by the cube-root of the larger volume.

value of the burning velocity. To minimize the influence of buoyancy, our models were fitted to an initial part of the experimental pressure curves on the basis of the following considerations.

Sapko, Furno, and Kuchta, 1976 studied the effect of buoyancy on methane–air–nitrogen flames in a 12-ft diameter spherical explosion vessel. They observed that the velocity of the geometric center of the rising flame ball increased with time according to

$$v_c = 117t^{0.44} \text{ cm s}^{-1}. \quad (83)$$

Using this correlation, one finds a shift of the geometric center (i.e. $\Delta y = 81t^{1.44}$) of about 0.1 cm in 10 ms, 1 cm in 50 ms, 3 cm in 100 ms, and 8 cm in 200 ms. These displacements obviously become significant in comparison with the radius of the 20-l sphere (17 cm) at later times.

A rising flame ball also has a tendency to change its shape because the movement of the upper half of the flame is assisted by buoyancy, while that of the lower part is being counteracted. As a result, the upper part of the flame maintains its spherical curvature, while the lower hemispherical part tends to flatten out. When v_c is larger than the flame speed, the lower hemispherical part of the flame may even change its shape from convexity towards the unburnt mixture into concavity. This continual change in the shape of the flame undermines the assumption of a spherical flame surface in the thin-flame and the three-zone model. Sapko et al. (1976) observed that the radius of the flame ball grows in time as

$$\gamma_{\text{flame}} = 354t^{1.13} \text{ cm}. \quad (84)$$

From this information and Eq. (83) one finds the following values for the flame speed and the rising velocity as a function of time: 220 and 15 cm s^{-1} at 10 ms, 270 and 31 cm s^{-1} at 50 ms, 297 and 42 cm s^{-1} at 100 ms, and 325 and 58 cm s^{-1} at 200 ms.

With the above estimations in mind, it was decided to fit the thin-flame model and the three-zone model to the part of the experimental curves where the pressure changed from 1.2 to 3.0 bar. The models were fitted to the experimental data by means of the Levenberg–Marquardt method (Marquardt, 1963; Press, Teukolsky, Vetterling, & Flannery, 1992). More specifically, the routine mrqmin by Press et al. was extended to enable the fitting of a differential equation by its numerical solution to a set of discrete data points. The numerical solution of the differential equations that constitute the thin-flame and the three-zone model was calculated by means of a fourth order Runge–Kutta method, using the routine rkdumb by the same authors.

For the thin-flame model, Eqs. (19) and (23) were used to describe the effect pressure and temperature on the laminar burning velocity and the optimal values of $\mathbf{S}_{uL}^{\circ}$ and β_2 were sought. Redundancy in the degrees of freedom was avoided by keeping β_1 at a fixed value of 1.89. For the three-zone model, Eqs. (76) and (77) were used to describe the dependence of the laminar burning velocity and the laminar flame thickness on pressure and temperature. The optimal values of $\mathbf{S}_{uL}^{\circ}$, c and α were sought by fitting the three-zone model to the experimental pressure–time curves. The reference laminar flame thickness, δ_L°, however, was kept at a fixed value of 1.0 mm.

The upper-left part of Fig. 7 shows a comparison between the predicted pressure curves and the experimental data of a stoichiometric methane–air explosion. The model curves are seen to be in good agreement with the experimental data and the corresponding results of the fit are shown in Table 2. With both integral balance models, the regression analysis yields a value of about 40–41 cm s^{-1} for the initial laminar burning velocity, $\mathbf{S}_{uL}^{\circ}$, which is within the scatter of values reported by other researchers: 42 cm s^{-1} (Andrews & Bradley, 1972), 38 cm s^{-1} (Bradley, Gaskell, & Gu, 1996), 40 cm s^{-1} (Law, 1993: Chapter 2) and 37 cm s^{-1} (van Maaren, Thung, & de Goey, 1994). The optimal value of β_2 in Eq. (19) is about -0.36, which is close to the expected value of -0.28 and within the range from -0.40 to -0.15. In case of Eq. (19), β_2 assumed a value of -0.46, which is close to the expected value of -0.41 and within the range from -0.60 to -0.20. The values of c and α, namely, -0.27 and -0.52, are also close to the expected values of 0.25 and 0.5. These values are also within the error bands discussed in Section 5. All experimental pressure–time curves were processed in this manner and the results are presented in Figs. 7 and 8. The corresponding numerical values with error estimates are shown in Tables 5 and 6.

The lower-left part of Fig. 7 shows the laminar burning velocity as a function of the equivalence ratio. The shaded region represents the band of data shown in Fig. 3 and the markers correspond to the laminar burning velocity obtained by fitting the thin-flame model and the three-zone model. For the entire range of equivalence ratios investigated, our results are seen to be within the band of data reported by other researchers. Although scatter may be observed in our data, there appears to be no systematic difference between laminar burning velocities obtained on the basis of Eqs. (19),(23), or (76). It appears to arise from the scatter in the experimental pressure–time curves (compare the scatter of the laminar burning velocity at a particular equivalence ratio with the difference between the corresponding experimental pressure–time curves).

The value of β_2 in Eqs. (19) and (23) appears to be decreasing as a function of the equivalence ratio and all values fall within the band of uncertainty (see the upper part of Fig. 8). When the following model is fitted to the data in the upper-left part of the figure,

$$\beta_2 = a_0 + a_1(\phi - 1), \quad (85)$$

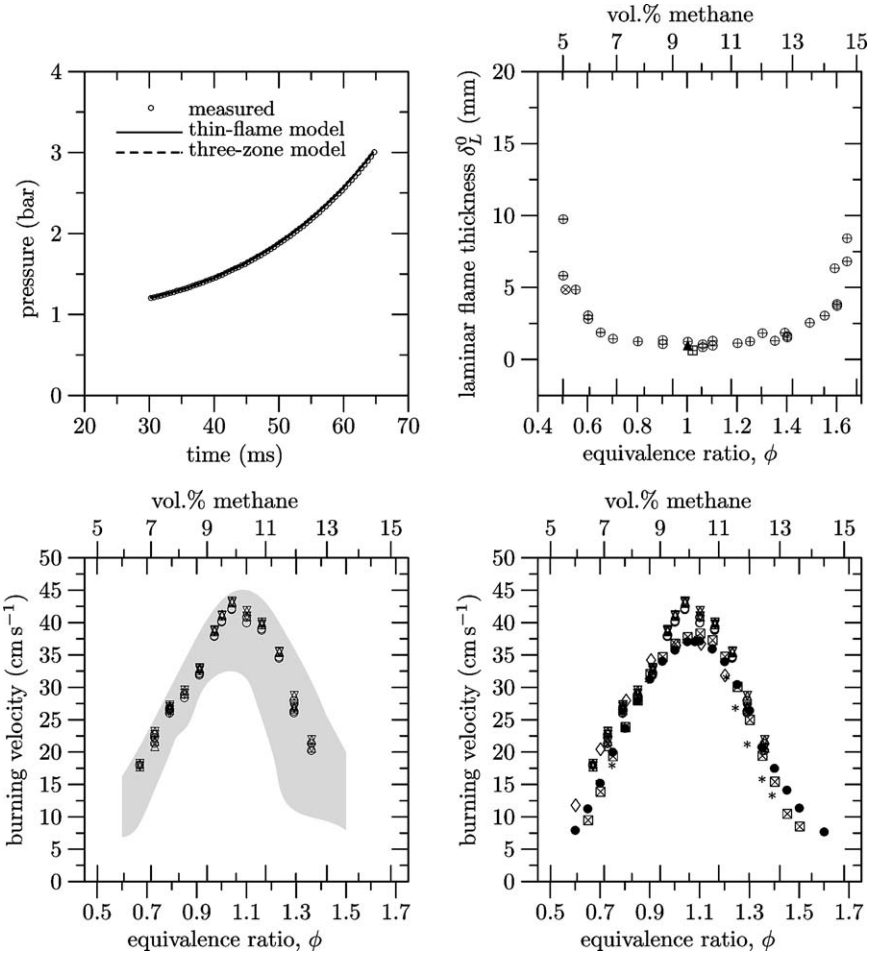

Fig. 7. Upper left: Correspondence between the model predictions and the experimental pressure curve for a stoichiometric methane–air mixture. Upper right: Laminar flame thicknesses from the literature. Lower left: Comparison between our laminar burning velocities and literature data. Lower right: Comparison between our values and recent data. ⊕ Andrews and Bradley (1972), ⊗ Dixon-Lewis and Williams (1967), ▲ Janisch (from Andrews and Bradley, 1972), ⊞ Dixon-Lewis and Wilson (1951), ⊠ van Maaren et al. (1994), ● Bosschaart and de Goey (2003), ◇ Gu et al. (2000), ∗ Vagelopoulos and Egolfopoulos (1998). ○ thin-flame model with Eq. (19), ▽ thin-flame model with Eq. (23), △ three-zone model with Eq. (76).

Table 2
Optimal values of the various degrees of freedom in thin-flame and the three-zone model

Parameter	Value ± StdErr		
	Thin-flame model		Three-zone model
	Eq. (19)	Eq. (23)	Eqs. (76) and (77)
$\mathbf{S}_{uL}^{\circ}$ (× 10^4 m s^{-1})	4005.89 ± 13.30	4118.22 ± 17.47	4122.62 ± 17.49
δ_L° (× 10^3 m)	–	–	1.0 (fixed)
β_1 (× 10^3)	1.89 (fixed)	1.89 (fixed)	–
β_2 (× 10^3)	−357.42 ± 5.02	−459.12 ± 8.31	–
c (× 10^3)	–	–	272.57 ± 4.16
α (× 10^3)	–	–	522.55 ± 4.16

For a 95% confidence interval, multiply StdErr by 1.9793.

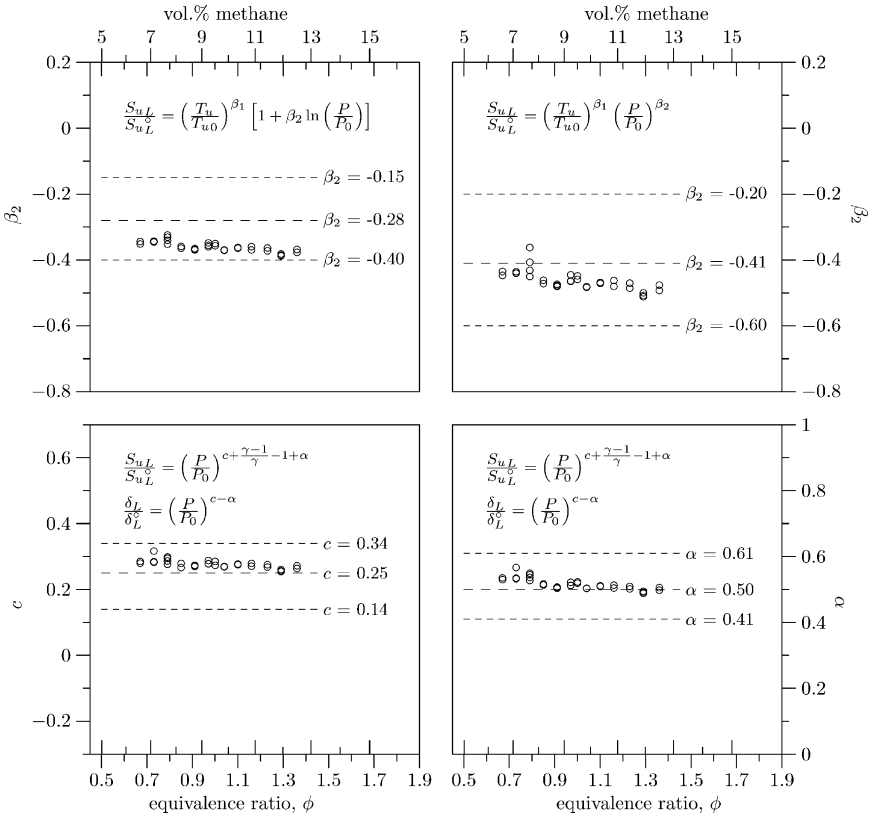

Fig. 8. Optimal value of the exponents β_2, α and c in Eqs. (19), (23) and (76), as a function of the equivalence ratio.

one finds that $a_0 = (-359.9 \pm 1.7) \times 10^{-3}$ and $a_1 = (-55.4 \pm 8.4) \times 10^{-3}$. These results are consistent with Eq. (21) as far as it concerns the value of a_0 and the decreasing trend with equivalence ratio. The value of a_1, however, appears to be about 20% of the slope of Eq. (21). An even greater discrepancy may be observed between the trend of the data in the upper-right part of Fig. 8 and Eq. (25): our data appear to decrease with increasing equivalence ratios while Eq. (25) suggests an increase. When Eq. (85) is fitted to these data one finds that $a_0 = (-461.3 \pm 4.2) \times 10^{-3}$ and $a_1 = (-10.7 \pm 2.0) \times 10^{-2}$.

The laminar flame thickness at reference conditions, δ_L°, was kept at a constant value of 1 mm in the application of the three-zone model to the experimental explosion curves. This value was chosen on the basis of observations reported by other researchers (see the upper-right part of Fig. 7) and the resulting laminar burning velocity is close to those obtained with the thin-flame model (see Table 2). The lower part of Fig. 8 indicates that the optimal values of c and α are close to the estimates made in the previous section. It should be emphasized that, in spite of the fact that the laminar burning velocities found in the present work appear to be within the band of data collected from the literature, far better methods are available to determine this quantity. This becomes evident when our results are compared with recent data on the laminar burning velocity of methane–air mixtures which are currently believed to be the correct ones (see the lower-right part of Fig. 7). Obviously, our laminar burning velocities are systematically higher and this discrepancy is most severe when the stoichiometric limit is approached. At the stoichiometric concentration our method gives a laminar burning velocity of 41–42 cm s^{-1}. The methods used by other researchers indicate a value of 37 cm s^{-1}. The cause of this discrepancy is due to the fact that the experimental information used by our method is too limited to compensate problems arising from buoyancy, flame front instability, and flame stretch. Additional measurements of flame position and flame shape would be necessary to improve the accuracy.

The sensitivity of the degrees of freedom in Eqs. (76) and (77) was investigated by varying the flame thickness and the results are presented in Table 3. It is seen that a change in the laminar flame thickness by a factor of 8 is accompanied by a negligible change in the other degrees of freedom. This low sensitivity to variations in δ_L° is caused by the fact that the volume occupied by the flame zone is small in comparison with that of the explosion vessel. As a result, variations in the thickness of the flame zone have little effect on the overall pressure. This low sensitivity is also reflected by the inaccuracy in the flame thickness when it is fitted as a degree of freedom. Table 4 shows the behavior of the inaccuracy in the flame thickness when the three-zone model is

Table 3
Effect of flame thickness on the optimal values of the degrees of freedom in Eqs. (76) and (77)

Fixed	Value ± StdErr		
δ_L° (× 10^3 m)	$\mathbf{S}_{uL}^\circ$ (× 10^4 m s^{-1})	c (× 10^3)	α (× 10^3)
0.5	4122.59 ± 17.49	272.57 ± 4.16	522.55 ± 4.16
1.0	4122.62 ± 17.49	272.57 ± 4.16	522.55 ± 4.16
2.0	4122.62 ± 17.49	272.56 ± 4.16	522.56 ± 4.16
4.0	4123.16 ± 17.49	272.51 ± 4.16	522.52 ± 4.15

For a 95% confidence interval, multiply StdErr by 1.9793.

Table 4
Accuracy of the optimal value of the laminar flame thickness in the three-zone model

Value ± StdErr		Fixed	
δ_L° (× 10^5 m)	$\mathbf{S}_{uL}^\circ$ (× 10^4 m s^{-1})	c (× 10^3)	α (× 10^3)
35.61 ± 14835.82	4122.59	272.57	522.55
101.96 ± 51.81	4122.62	272.57	522.55
203.27 ± 25.99	4122.62	272.56	522.56
398.06 ± 13.27	4123.16	272.51	522.52

For a 95% confidence interval, multiply StdErr by 1.9793.

fitted to the experimental pressure–time curve with the optimal values of $\mathbf{S}_{uL}^\circ$, c and α from Table 3 as constants. Ideally, one would expect laminar flame thicknesses which are close to the ones shown in Table 3, with a small degree of uncertainty. It is seen, however, that the optimal value in Table 4 which corresponds to a flame thickness of 0.5 mm deviates by about 30%. The uncertainty is a factor of 400 larger than the optimal flame thickness itself. Both the deviation of the optimal flame thickness as well as the uncertainty appears to decrease significantly as the flame thickness becomes larger. With a flame thickness of 4 mm, the deviation is less than 0.5% from the expected value and the uncertainty is about 3%.

7. Conclusions

The potential of the idea of finding the laminar burning velocity of a combustible mixture by fitting the integral balance models of DZLS to the experimental pressure–time curve of an explosion in a closed vessel was explored. The conclusions arising from this investigation are summarized as follows.

Because the laminar burning velocity and the laminar flame thickness are known to depend pressure and temperature, correlations have been sought to incorporate this sensitivity into the integral balance models. The thin-flame model required a correlation for the burning velocity only. A number of correlations proposed by other researchers have been reviewed and two, namely, Eqs. (19) and (23), were found to be suitable for the aim of the present work. The three-zone model required an additional expression for the effect of pressure and temperature on the flame thickness. Hence, a new set of correlations has been derived from first principles. These correlations, namely, one for the laminar burning velocity, Eq. (76), and one for the laminar flame thickness, Eq. (77), are strongly coupled because they have two degrees of freedom, c and α, in common. This coupling arises from first principles and appears to be of crucial importance: it was observed that redundancy occurred in its absence (i.e. if the exponents $c + (\gamma-1)/\gamma-1 + \alpha$ and $c-\alpha$ were replaced by totally independent degrees of freedom).

To verify the methodology proposed in this work, a number of methane–air explosions were carried out in a 20-l sphere. The equivalence ratio was varied between 0.67 and 1.36, and the pressure–time curve was measured. Explosion severity parameters which are commonly used as a design basis for the protection and suppression of accidental explosions (P_{max} and $(dP/dt)_{max}$) were determined from these curves and compared with results reported by other researchers. While good agreement exists between our findings and those of Cashdollar and Hertzberg with off-stoichiometric mixtures, an increasing discrepancy may be observed when the stoichiometric limit is approached from either side. With stoichiometric mixtures, a difference of 6% is observed in the value of P_{max} and a difference of 13% in case of

Table 5
Optimal values of the degrees of freedom in Eqs. (19) and (23). The parameter β_1 was kept at a fixed value of 1.89

No.	ϕ	$\frac{S_{uL}}{S^{\circ}_{uL}} = \left(\frac{T_u}{T_{u0}}\right)^{\beta_1}\left[1 + \beta_2 \ln\left(\frac{P}{P_0}\right)\right]$		$\frac{S_{uL}}{S^{\circ}_{uL}} = \left(\frac{T_u}{T_{u0}}\right)^{\beta_1}\left(\frac{P}{P_0}\right)^{\beta_2}$	
		$S^{\circ}_{uL} \pm \text{StdErr} \times 10^4$ (m/s)	$\beta_2 \pm \text{StdErr} \times 10^3$	$S^{\circ}_{uL} \pm \text{StdErr} \times 10^4$ (m/s)	$\beta_2 \pm \text{StdErr} \times 10^3$
52	0.67	1749.79 ± 3.25	−351.64 ± 3.00	1798.65 ± 4.18	−447.00 ± 4.78
53	0.67	1798.82 ± 3.40	−344.37 ± 2.91	1837.11 ± 4.40	−435.10 ± 4.71
44	0.73	2130.91 ± 4.80	−343.10 ± 3.43	2185.66 ± 6.23	−436.20 ± 5.56
46	0.73	2224.70 ± 4.96	−345.82 ± 3.41	2282.02 ± 6.44	−440.04 ± 5.54
48	0.73	2270.46 ± 5.25	−345.35 ± 3.50	2330.27 ± 6.84	−440.33 ± 5.70
31	0.79	2652.15 ± 7.15	−324.20 ± 4.11	2713.74 ± 9.15	−407.31 ± 6.49
32	0.79	2668.74 ± 7.04	−330.86 ± 4.06	2619.51 ± 8.78	−362.34 ± 6.51
33	0.79	2673.74 ± 6.82	−340.65 ± 3.91	2740.32 ± 8.82	−431.78 ± 6.31
36	0.79	2597.71 ± 6.56	−352.39 ± 3.86	2667.32 ± 8.56	−450.43 ± 6.32
54	0.85	2837.13 ± 7.74	−364.76 ± 4.06	2992.10 ± 10.26	−472.25 ± 6.82
55	0.85	2887.37 ± 7.85	−359.34 ± 4.12	2968.81 ± 10.32	−462.08 ± 6.83
56	0.91	3208.13 ± 9.42	−367.88 ± 4.34	3307.04 ± 12.54	−478.01 ± 7.36
57	0.91	3214.29 ± 9.33	−369.63 ± 4.28	3314.58 ± 12.44	−481.04 ± 7.28
58	0.91	3186.72 ± 9.04	−366.02 ± 4.23	3282.26 ± 12.00	−474.25 ± 7.13
41	0.97	3793.39 ± 11.71	−360.72 ± 4.68	3902.01 ± 15.43	−465.03 ± 7.79
42	0.97	3784.19 ± 12.12	−348.77 ± 4.88	3884.44 ± 15.80	−445.23 ± 7.97
43	0.97	3791.04 ± 11.94	−359.97 ± 4.73	3900.24 ± 15.74	−464.17 ± 7.88
59	1.00	4005.89 ± 13.30	−357.42 ± 5.02	4118.22 ± 17.47	−459.12 ± 8.31
60	1.00	4021.17 ± 13.23	−350.31 ± 4.97	4130.43 ± 17.30	−448.52 ± 8.16
63	1.04	4197.14 ± 13.74	−370.05 ± 4.87	4327.18 ± 18.36	−481.43 ± 8.25
64	1.04	4212.66 ± 13.76	−370.90 ± 4.83	4345.10 ± 18.37	−483.45 ± 8.22
61	1.10	3993.67 ± 12.95	−364.27 ± 4.83	4112.00 ± 17.15	−471.28 ± 8.12
62	1.10	4076.82 ± 13.25	−362.53 ± 4.85	4197.12 ± 17.54	−468.84 ± 8.13
67	1.16	3880.17 ± 12.53	−359.83 ± 4.85	3989.73 ± 16.50	−462.86 ± 8.08
68	1.16	3900.24 ± 12.45	−369.73 ± 4.73	4019.88 ± 16.58	−480.43 ± 8.03
65	1.23	3448.52 ± 10.47	−372.23 ± 4.44	3558.52 ± 13.99	−485.79 ± 7.59
66	1.23	3467.06 ± 10.62	−363.57 ± 4.52	3570.41 ± 14.09	−470.53 ± 7.6
69	1.29	2603.96 ± 6.44	−385.85 ± 3.61	2692.46 ± 8.72	−507.93 ± 6.30
70	1.29	2794.47 ± 7.32	−381.56 ± 3.85	2886.31 ± 9.86	−500.08 ± 6.65
71	1.29	2628.80 ± 6.51	−387.93 ± 3.61	2720.02 ± 8.84	−512.07 ± 6.32
72	1.36	2022.39 ± 4.25	−368.16 ± 3.14	2082.69 ± 5.65	−476.68 ± 5.30
73	1.36	2134.94 ± 4.64	−377.51 ± 3.21	2203.17 ± 6.23	−493.01 ± 5.51

$(dP/dt)_{max}$. When our results are compared with those of Bartknecht, a smaller discrepancy exists in P_{max}, but a larger difference may be observed in the maximum rate of pressure rise. We found a K_G value of 80 bar m s^{-1} while Bartknecht measured a value of 55 bar m s^{-1}. The practical consequence of this observation is that explosion hazards are systematically being underestimated because a K_G value of 55 bar m s^{-1} is widely believed to be the correct explosion severity index of stoichiometric methane–air mixtures.

The thin-flame model and the three-zone model were fitted to the pressure–time curves of the methane–air explosions and the laminar burning velocity was determined as a function of equivalence ratio. Our laminar burning velocities are found to be within the data band of those reported by other researchers (see Fig. 7). The scatter in our laminar burning velocities arising from the use of two different integral balance models, as well as the incorporation of a variety of correlations (i.e. Eqs. (19),(23) and (76)), appears to be insignificant in comparison with the scatter caused by the variation between pressure–time curves measured at one particular equivalence ratio. The optimal value of β_2 in Eqs. (19) and (23), as well as that of c and α in Eqs. (76) and (77), are also seen to be in agreement with estimates made on the basis of literature data (see Fig. 8).

It was discussed in the previous section that, although our laminar burning velocities appear to fall within the data band of values reported by other researchers, the method explored in the present work should not be the first choice if one desires to know the laminar burning velocity of a combustible mixture. In fact, it should only be used when there is no better alternative. This may be the case, for example, when an estimate is sought of the laminar burning velocity of a dust–air mixture, a combustible spray, or a toxic gas mixture with unfavorable optical properties.

There appeared to be a large uncertainty in the optimal value of the laminar flame thickness which was attributed to the fact that the laminar flame thickness of the

Table 6
Optimal values of the degrees of freedom in Eqs. (76) and (77). The laminar flame thickness at reference conditions, δ_L°, was kept at a fixed value of 1.0 mm

No.	ϕ	$\frac{S_{uL}}{S_{uL}^\circ} = \left(\frac{P}{P_0}\right)^{c+(\gamma-1)/\gamma-1+\alpha}$ and $\frac{\delta_L}{\delta_L^\circ} = \left(\frac{P}{P_0}\right)^{c-\alpha}$		
		$S_{uL}^\circ \pm$ StdErr $\times 10^4$ (m/s)	$c \pm$ StdErr $\times 10^3$	$\alpha \pm$ StdErr $\times 10^3$
52	0.67	1797.09 ± 4.23	279.54 ± 2.31	529.53 ± 2.31
53	0.67	1837.13 ± 4.40	284.59 ± 2.35	534.59 ± 2.35
44	0.73	2185.68 ± 6.23	284.04 ± 2.78	534.04 ± 2.78
46	0.73	2109.62 ± 5.83	316.26 ± 2.73	566.30 ± 2.73
48	0.73	2330.29 ± 6.84	281.90 ± 2.85	531.97 ± 2.85
31	0.79	2713.76 ± 9.15	298.49 ± 3.24	548.48 ± 3.24
32	0.79	2731.63 ± 9.03	293.88 ± 3.23	543.87 ± 3.23
33	0.79	2740.34 ± 8.82	286.25 ± 3.16	536.25 ± 3.16
36	0.79	2667.34 ± 8.56	276.93 ± 3.16	526.92 ± 3.16
54	0.85	2922.12 ± 10.26	266.02 ± 3.41	516.01 ± 3.41
55	0.85	2968.81 ± 10.32	279.12 ± 3.42	513.09 ± 3.42
56	0.91	3307.07 ± 12.54	271.15 ± 3.68	505.12 ± 3.68
57	0.91	3314.61 ± 12.44	269.64 ± 3.64	505.59 ± 3.64
58	0.91	3282.29 ± 12.00	273.03 ± 3.57	507.00 ± 3.57
41	0.97	3902.04 ± 15.43	277.66 ± 3.90	511.60 ± 3.90
42	0.97	3884.48 ± 15.80	287.54 ± 3.99	521.51 ± 3.99
43	0.97	3900.27 ± 15.74	278.08 ± 3.94	512.04 ± 3.94
59	1.00	4122.62 ± 17.49	272.57 ± 4.16	522.55 ± 4.16
60	1.00	4145.38 ± 17.33	284.56 ± 4.08	518.53 ± 4.08
63	1.04	4327.22 ± 18.31	269.44 ± 4.13	503.41 ± 4.13
64	1.04	4345.14 ± 18.37	268.44 ± 4.11	502.40 ± 4.11
61	1.10	4112.03 ± 17.15	274.51 ± 4.06	508.49 ± 4.06
62	1.10	4192.40 ± 17.52	276.47 ± 4.07	510.44 ± 4.07
67	1.16	3989.77 ± 16.50	278.71 ± 4.04	512.71 ± 4.04
68	1.16	4019.91 ± 16.58	269.94 ± 4.02	503.92 ± 4.02
65	1.23	3558.55 ± 13.99	267.26 ± 3.74	501.23 ± 3.79
66	1.23	3570.45 ± 14.09	274.88 ± 3.81	508.86 ± 3.81
69	1.29	2692.48 ± 8.72	256.18 ± 3.15	490.17 ± 3.15
70	1.29	2886.34 ± 9.86	260.11 ± 3.33	494.09 ± 3.33
71	1.29	2720.04 ± 8.84	254.12 ± 3.16	488.09 ± 3.16
72	1.36	2083.89 ± 5.65	271.44 ± 2.65	505.42 ± 2.65
73	1.36	2203.18 ± 6.30	263.64 ± 2.76	497.63 ± 2.76

investigated mixtures is small in comparison with the radius of the 20-l sphere. It has also been observed that the uncertainty decreased to acceptable proportions when the flame thickness was increased to about 2% of the radius of the vessel (see Table 4). This implies that a 20-l explosion sphere is unsuitable if one desires to determine the laminar flame thickness of methane–air mixtures with the methodology presented in this paper. An explosion vessel with a radius of no more than 50 times the laminar flame thickness would have to be used.

References

Agnew, J. T., & Graiff, L. B. (1961). The pressure dependence of laminar burning velocity by the spherical bomb method. *Combustion and Flame, 5*, 209–219.

Andrews, G. E., & Bradley, D. (1972). The burning velocity of methane–air mixtures. *Combustion and Flame, 19*, 275–288.

Babkin, V. S., and Kozachenko, L. S. (1966). Study of normal burning velocity in methane–air mixtures at high pressures. *Fizika Goreniya i Vzryva, 2*(3), 77–86 (English translation: *Combustion, Explosion and Shock Waves, 2*, 46–52).

Babkin, V. S., Kozachenko, L. S., & Kuznetsov, I. L. (1964). The effect of pressure on the normal burning velocity of a methane–air mixture. *Zhurnal Prikladnoi Mekhaniki i Tekhnicheskoi Fizika, 3*, 145–149 (English translation in 1966 by Scripta Technica, Inc., 275 Madison Avenue, New York 16, NY. Translated for the US Department of the Interior, Bureau of Mines, Washington, DC).

Barassin, A., Lisbet, R., Combourieu, J., & Laffitte, P. (1967). Etude de l'influence de la temperature initiale sur la vitesse normale de deflagration de melanges methane–air en fonction de la concentration. *Bulletin de la Societe Chimique de France, 104*(7), 2521–2526.

Bartknecht, W. (1981). *Explosions: Course prevention protection*. Springer Verlag (Translation of Burg, H., and Almond, T. *Explosionen, Ablauf und Schutzmaβnahmen* (2nd ed.)).

Bosschaart, K. J., & de Goey, L. P. H. (2003). Detailed analysis of the heat flux method for measuring burning velocities. *Combustion and Flame, 132*, 170–180.

Bradley, D., Cresswell, T. M., & Puttock, J. S. (2001). Flame acceleration due to flame-induced instabilities in large-scale explosions. *Combustion and Flame, 124*, 551–559.

Bradley, D., Gaskell, P. H., & Gu, X. J. (1996). Burning velocities, Markstein lengths, and flame quenching for spherical methane–air flames: a computational study. *Combustion and Flame*, *104*, 176–198.

Bradley, D., & Harper, C. M. (1994). The development of instabilities in laminar explosion flames. *Combustion and Flame*, *99*, 562–572.

Bradley, D., Hicks, R. A., Lawes, M., Sheppard, C. G. W., & Woolley, R. (1998). The measurement of laminar burning velocities and Markstein numbers for iso-octane–air and iso-octane–*n*-heptane–air mixtures at elevated temperatures and pressures in an explosion bomb. *Combustion and Flame*, *115*, 126–144.

Bradley, D., and Hundy, G. F., Burning velocities of methane–air mixtures using hot-wire anemometers in closed-vessel explosions. In Proceedings of the Thirteenth Symposium (International) on Combustion (pp. 575–583). The Combustion Institute, 1971.

Bradley, D., Sheppard, C. G. W., Woolley, R., Greenhalgh, D. A., & Lockett, R. D. (2000). The development and structure of flame instabilities and cellularity at low Markstein numbers in explosions. *Combustion and Flame*, *122*, 195–209.

Cashdollar, K. L., & Hertzberg, M. (1985). 20-l Explosibility test chamber for dusts and gases. *Review of Scientific Instruments*, *56*(4), 596–602.

Clarke, A., Stone, R., & Beckwith, P. (1995). Measuring the laminar burning velocity of methane–diluent–air mixtures within a constant-volume combustion bomb in a micro-gravity environment. *Journal of the Institute of Energy*, *68*(September), 130–136.

Clingman, W. H., Brokaw, R. S., and Pease, R. N., Burning velocities of methane with nitrogen-oxygen, argon-oxygen and helium-oxygen mixtures. In Proceedings of the Fourth Symposium (International) on Combustion (pp. 310–313). The Combustion Institute, 1953.

Clingman, W. H., & Pease, R. N. (1956). Critical considerations in the measurements of burning velocities of bunsen burner flames and interpretation of the pressure effect. Measurements and calculations for methane. *Journal of the American Chemical Society*, *78*(9), 1775–1780.

Dahoe, A. E. (2000). *Dust explosions: A study of flame propagation*. Ph. D. Thesis, Delft University of Technology, May.

Dahoe, A. E., Cant, R. S., Pegg, M. J., & Scarlett, B. (2001). On the transient flow in the 20-liter explosion sphere. *Journal of Loss Prevention in the Process Industries*, *14*, 475–487.

Dahoe, A. E., van der Nat, K., Braithwaite, M., & Scarlett, B. (2001). On the sensitivity of the maximum explosion pressure of a dust deflagration to turbulence. *KONA Powder and Particle*, *19*, 178–196.

Dahoe, A. E., van Velzen J., Sluijs, L. P., Neervoort, F. J., Leschonski, S., Lemkowitz, S. M., van der Wel, P. G. J., and Scarlett, B., Construction and operation of a 20-litre dust explosion sphere at and above atmospheric conditions. In J. J., Mewis, H. J. Pasman, and E. E. De Rademaeker, editors, *Loss Prevention and Safety Promotion in the Process Industries, Proceedings of the 8th International Symposium*, Vol. 2, pp. 285–302. European Federation of Chemical Engineering (EFCE), Elsevier Science, 1995.

Dahoe, A. E., Zevenbergen, J. F., Lemkowitz, S. M., & Scarlett, B. (1996). Dust explosions in spherical vessels: the role of flame thickness in the validity of the 'cube-root-law'. *Journal of Loss Prevention in the Process Industries*, *9*, 33–44.

Diederichsen, J., & Wolfhard, H. G. (1956). The burning velocity of methane flames at high pressure. *Transactions of the Faraday Society*, *52*, 1102–1109.

Dixon-Lewis, G., & Williams, A. (1967). *The combustion of CH_4* in premixed flames. In Proceedings of the eleventh symposium (international) on combustion. (p. 951). The Combustion Institute.

Dixon-Lewis, G., & Wilson, J. G. (1951). A method for the measurement of the temperature distribution in the inner cone of a Bunsen flame. *Transactions of the Faraday Society*, *46*, 1106–1114.

Dryer, F. L., & Glassman, I. (1972). *High temperature oxidation of CO and CH_4*. In Proceedings of the fourteenth symposium (international) on combustion. (pp. 987–1003). The Combustion Institute.

Dugger, G. L. (1952). *Effect of initial mixture temperature on flame speed of methane–air, propane–air and ethylene–air mixtures*. NACA report of investigations 1061, Lewis Flight Propulsion Laboratory, Cleveland, OH, 1952.

Edmondson, H., & Heap, M. P. (1969). The burning velocity of methane–air flames inhibited by methyl bromide. *Combustion and Flame*, *13*, 472–478.

Edmondson, H., & Heap, M. P. (1970). Ambient atmosphere effects in flat-flame measurements of the burning velocity. *Combustion and Flame*, *14*, 195–202.

Egerton, A., & Lefebvre, A. H. (1954). Flame propagation: the effect of pressure variation on burning velocities. *Proceedings of the Royal Society of London, Series A: Mathematical and Physical Sciences*, *222*, 206–223.

Egolfopoulos, F. N., Cho, P., & Law, C. K. (1989). Laminar flame speeds of methane–air mixtures under reduced and elevated pressures. *Combustion and Flame*, *76*, 375–391.

Gibbs, G. J., & Calcote, H. F. (1959). Effect of molecular structure on burning velocity. *Journal of Chemical and Engineering Data*, *4*(3), 226–237.

Gilbert, M. (1957). *The influence of pressure on flame speed*. In Proceedings of the sixth symposium (international) on combustion. (pp. 74–83). The Combustion Institute.

Gu, X. J., Haq, M. Z., Lawes, M., & Woolley, R. (2000). Laminar burning velocities and Markstein lengths of methane–air mixtures. *Combustion and Flame*, *121*, 41–58.

Günther, R., & Janisch, G. (1972). Measurements of burning velocity in a flat flame front. *Combustion and Flame*, *19*, 49–53.

Halpern, C. (1958). Measurement of flame speed by a nozzle burner method. *Journal of Research of the National Bureau of Standards*, *60*(6), 535–546.

Haq, M. Z., Sheppard, C. G. W., Woolley, R., Greenhalgh, D. A., & Lockett, R. D. (2002). Wrinkling and curvature of laminar and turbulent premixed flames. *Combustion and Flame*, *131*, 1–15.

Iijima, T., & Takeno, T. (1986). Effects of temperature and pressure on burning velocity. *Combustion and Flame*, *65*, 35–43.

Johnston, W. C. (1947). W.C. Johnston measures flame velocity of fuels at low pressures. *Society of Automotive Engineers Journal*, *55*(December), 62–65.

Lees, F. P. (1996). *Loss prevention in the process industries; hazard identification, assessment and control*. Guilford: Butterworth-Heinemann.

Karpov, V. P., & Sokolik, A. S. (1961). Relation between spontaneous ignition and laminar and turbulent burning velocities of paraffin hydrocarbons. *Doklady Akademii Nauk USSR*, *138*(4), 874–876.

Kawakami, T., Okajima, S., & Iinuma, K. (1988). *Measurement of slow burning velocity by zero-gravity method*. In Proceedings of the twenty-second symposium (international) on combustion. (pp. 1609–1613). The Combustion Institute.

Kuo, K. K. (1986). *Principles of combustion*. New York: John Wiley & Sons.

Law, C. K. (1993). A compilation of experimental data on laminar burning velocities. In N. Peters, & B. Rogg (Eds.), *Reduced kinetic mechanisms for applications in combustion systems* (pp. 15–26). *Lecture notes in physics*, Vol. 19. Springer Verlag.

Lindow, R. (1968). Eine verbesserte Brennermethode zur Bestimmung der laminaren Flammenge-schwindigkeiten von Brenngas/luftgemischen. *Brennstoff, Wärme, Kraft*, *20*(1), 8–14.

Manton, J., & Milliken, B. B. (1956). *Study of pressure dependence of burning velocity by the spherical vessel method*. In Proceedings of the gas dynamics symposium on aerothermochemistry. (pp. 151–157). Illinois: Northwestern University.

Marquardt, D. W. (1963). An algorithm for least-squares estimation

of nonlinear parameters. *SIAM Journal on Applied Mathematics*, *11*, 431–441.

Metghalchi, M., & Keck, J. C. (1982). Burning velocities of mixtures of air with methanol isooctane, and indolene at high pressure and temperature. *Combustion and Flame*, *48*, 191–210.

Perlee, H. E., Fuller, F. N., and Saul, C. H. (1974). *Constant-volume flame propagation*. Report of investigations 7839, US Department of the Interior, Bureau of Mines, Washington, DC.

Press, W. H., Teukolsky, S. A., Vetterling, W. T., & Flannery, B. P. (1992). *Numerical recipes in PASCAL. The art of scientific computing* (2nd ed.). Cambridge: Cambridge University Press.

Reed, S. B., Mineur, J., & McNaughton, J. P. (1971). The effect on the burning velocity of methane of vitiation of combustion air. *Journal of the Institute of Fuel*, *155*(March), 149–155.

Sapko, M. J., Furno, A. L., and Kuchta, J. M. (1976). *Flame and pressure development of large-scale CH_4–air–N_2 explosions*. Report of investigations 8176, US Department of the Interior, Bureau of Mines, Washington, DC.

Scholte, T. G., & Vaags, P. B. (1959). The burning velocity of hydrogen–air mixtures and mixtures of some hydrocarbons with air. *Combustion and Flame*, *3*, 495–501.

Senecal, J. A., & Beaulieu, P. A. (1998). K_G: new data analysis. *Process Safety Progress*, *17*, 9–15.

Sharma, S. P., Agrawal, D. D., & Gupta, C. P. (1981). *The pressure and temperature dependence of burning velocity in a spherical combustion bomb*. In Proceedings of the eighteenth symposium (international) on combustion. (pp. 493–501). The Combustion Institute.

Singer, J. M., Grumer, J., & Cook, E. B. (1956). *Burning velocities by the Bunsen-burner method I. Hydrocarbon–oxygen mixtures at one atmosphere. II. Hydrocarbon–air mixtures at subatmospheric pressures*. In Proceedings of the gas dynamics symposium on aerothermochemistry. (pp. 139–150). Illinois: Northwestern University.

Smith, D., & Agnew, J. T. (1951). *The effect of pressure on the laminar burning velocity of methane–oxygen–nitrogen mixtures*. In Proceedings of the sixth symposium (international) on combustion. (pp. 83–88). The Combustion Institute.

Spalding, D. B. (1979). *Combustion and mass transfer*. New York: Pergamon.

Strauss, W. A., & Edse, R. (1959). *Burning velocity measurements by the constant pressure bomb method*. In Proceedings of the seventh symposium (international) on combustion. (pp. 377–385). The Combustion Institute.

Tsatsaronis, G. (1978). Prediction of propagating laminar flames in methane, oxygen, nitrogen mixtures. *Combustion and Flame*, *33*, 217–239.

Turns, S. R. (1996). *An introduction to combustion. McGraw-Hill series in mechanical engineering*. McGraw-Hill.

Vagelopoulos, C. M., & Egolfopoulos, F. N. (1998). *Direct experimental determination of laminar flame speeds*. In Proceedings of the twenty-seventh symposium (international) on combustion. (pp. 513–519). The Combustion Institute.

van Maaren, A., Thung, D. S., & De Goey, L. P. H. (1994). Measurement of flame temperature and adiabatic burning velocity of methane–air mixtures. *Combustion Science and Technology*, *96*, 327–344.

Vasserman, A. A., Kazavchinskii, Ya. Z., & Rabinovich, V. A. (1971). *Teplofizicheskie svoitva vozdukha i ego komponentov* [*Thermophysical properties of air and air components*]. Jerusalem: Israel Program for Scientific Translations, Ltd (Translated from Russian).

Warnatz, J. (1981). *The structure of laminar alkane-, alkene-, and acetylene flames*. In Proceedings of the eighteenth symposium (international) on combustion. (pp. 369–384). The Combustion Institute.

Williams, F. A. (1985). *Combustion theory* (2nd ed.). Addison-Wesley Publishing Company.

Wu, C. K., & Law, C. K. (1984). *On the determination of laminar flame speeds from stretched flames*. In Proceedings of the twentieth symposium (international) on combustion. (pp. 1941–1949). The Combustion Institute.